A CORROSION MONITORING SYSTEM FOR EXISTING REINFORCED CONCRETE STRUCTURES

Final Report

SPR 736

Oregon Department of Transportation

A CORROSION MONITORING SYSTEM FOR EXISTING REINFORCED CONCRETE STRUCTURES

Final Report

SPR 736

by
Xianming Shi, Ph.D., P.E.
Zhirui Ye, Ph.D.
Anburaj Muthumani, M.Sc.
Yan Zhang
Western Transportation Institute
Montana State University
And
James F. Dante
Hui Yu, Ph.D.
Southwest Research Institute

for

Oregon Department of Transportation
Research Section
555 13th Street NE, Suite 1
Salem OR 97301

and

Federal Highway Administration
400 Seventh Street, SW
Washington, DC 20590-0003

May 2015

Technical Report Documentation Page

1. Report No.	2. Government Accession No.	3. Recipient's Catalog No.
FHWA-OR-RD-15-14		

4. Title and Subtitle	5. Report Date
A Corrosion Monitoring System for Existing Reinforced Concrete Structures	-May 2015-
	6. Performing Organization Code

7. Author(s)	8. Performing Organization Report No.
Xianming Shi*, Zhirui Ye, Anburaj Muthumani, Yan Zhang, James F. Dante, Hui Yu	

9. Performing Organization Name and Address	10. Work Unit No. (TRAIS)
Western Transportation Institute Post Office Box 174250, Montana State University Bozeman, MT 59717-4250	11. Contract or Grant No. SPR 736

12. Sponsoring Agency Name and Address		13. Type of Report and Period Covered
Oregon Dept. of Transportation Research Section and 555 13th Street NE, Suite 1 Salem, OR 97301	Federal Highway Admin. 400 Seventh Street, SW Washington, DC 20590-0003	Final Report: 3/11 to 9/14 14. Sponsoring Agency Code

15. Supplementary Notes: *Principal Investigator is now with Washington State University. Xianming.Shi@wsu.edu

16. Abstract-

This study evaluated a multi-parameter corrosion monitoring system for existing reinforced concrete structures in chloride-laden service environments. The system was fabricated based on a prototype concrete corrosion measurement system that had been built and patented by Southwest Research Institute (SwRI).

In a laboratory benchmark test, a chloride concentration vs. potential calibration curve was established and indicated good linearity between 0.01 mol/L and 1 mol/L. The general and maximum localized corrosion rates, as measured by the Multi-electrode Array Sensor (MAS) probe, were all sensitive to the incremental chloride concentration in a simulated pore solution. However, once active corrosion is initiated and a great amount of chloride is present, the MAS probe may no longer serve as a good tool to predict the corrosion rate of rebar unless more research is conducted to establish such prediction or correlation. It was also revealed that in a sensor longevity test, only a fraction of sensors can be considered reliable after eight accelerated weathering cycles.

In addition, a laboratory pilot-scale test was done by incorporating an array of three sensing units at different depth of a mortar cylinder to monitor the ingress of chloride and the corrosion rate of rebar at different depths. The results identified many challenges to improve the sensor probe.

A detailed guideline along with video documentation was developed as a reference to guide field implementation. A field deployment of the system in an ODOT bridge pier was attempted for a few months. However, future research into improvements of the sensor system is needed to achieve a successful field application.

17. Key Words- bridge preservation, rebar, reinforced concrete, corrosion monitoring, chloride sensor, multi-electrode array sensor, field implementation	18. Distribution Statement Copies available from NTIS, and online at http://www.oregon.gov/ODOT/TD/TP_RES/

19. Security Classification (of this report)	20. Security Classification (of this page)	21. No. of Pages	22. Price
Unclassified	Unclassified	87	

SI* (MODERN METRIC) CONVERSION FACTORS

APPROXIMATE CONVERSIONS TO SI UNITS

Symbol	When You Know	Multiply By	To Find	Symbol
		LENGTH		
in	inches	25.4	millimeters	mm
ft	feet	0.305	meters	m
yd	yards	0.914	meters	m
mi	miles	1.61	kilometers	km
		AREA		
in^2	square inches	645.2	millimeters squared	mm^2
ft^2	square feet	0.093	meters squared	m^2
yd^2	square yards	0.836	meters squared	m^2
ac	acres	0.405	hectares	ha
mi^2	square miles	2.59	kilometers squared	km^2
		VOLUME		
fl oz	fluid ounces	29.57	milliliters	ml
gal	gallons	3.785	liters	L
ft^3	cubic feet	0.028	meters cubed	m^3
yd^3	cubic yards	0.765	meters cubed	m^3
NOTE: Volumes greater than 1000 L shall be shown in m^3.				
		MASS		
oz	ounces	28.35	grams	g
lb	pounds	0.454	kilograms	kg
T	short tons (2000 lb)	0.907	megagrams	Mg
		TEMPERATURE (exact)		
°F	Fahrenheit	(F-32)/1.8	Celsius	°C

APPROXIMATE CONVERSIONS FROM SI UNITS

Symbol	When You Know	Multiply By	To Find	Symbol
		LENGTH		
mm	millimeters	0.039	inches	in
m	meters	3.28	feet	ft
m	meters	1.09	yards	yd
km	kilometers	0.621	miles	mi
		AREA		
mm^2	millimeters squared	0.0016	square inches	in^2
m^2	meters squared	10.764	square feet	ft^2
m^2	meters squared	1.196	square yards	yd^2
ha	hectares	2.47	acres	ac
km^2	kilometers squared	0.386	square miles	mi^2
		VOLUME		
ml	milliliters	0.034	fluid ounces	fl oz
L	liters	0.264	gallons	gal
m^3	meters cubed	35.315	cubic feet	ft^3
m^3	meters cubed	1.308	cubic yards	yd^3
		MASS		
g	grams	0.035	ounces	oz
kg	kilograms	2.205	pounds	lb
Mg	megagrams	1.102	short tons (2000 lb)	T
		TEMPERATURE (exact)		
°C	Celsius	1.8C+32	Fahrenheit	°F

*SI is the symbol for the International System of Measurement

ACKNOWLEDGEMENTS

The research reported herein was financially supported by the Oregon Department of Transportation (ODOT) as well as the Research & Innovative Technology Administration (RITA) at the U.S. Department of Transportation (USDOT) through Alaska University Transportation Center (AUTC) and Western Transportation Institute (WTI). The authors are indebted to the ODOT project manager Steve Soltesz, AUTC project manager Billy Connor, and other technical panel members (Ray Bottenberg and James Garrard at ODOT, David Trejo and Kagan Tumer at Oregon State University, Tim Rogers at FHWA, et al.) for their continued support throughout this project. Part of the laboratory investigation (related to refinement and in-concrete testing of corrosion sensing system) undertaken by the SwRI team led by Dr. Hui Yu was under a subcontract with Montana State University. The authors also extend their appreciation to the following colleagues and students for their assistance to this research: Yongbo Yu, Yida Fang, Michelle Akin, Keith Fortune, Haokun Yu, Yang Xiong, Alexandra Pace, Nirap Sanju, and Emily Jackson.

DISCLAIMER

EXECUTIVE SUMMARY

This study evaluated a multi-parameter corrosion monitoring system for existing reinforced concrete structures in chloride-laden service environments. The system was fabricated based on a prototype concrete corrosion measurement system that had been built and patented by Southwest Research Institute (SwRI). The sensor was configured with an array of three sensing units at different positions along its length, which facilitate the ability to monitor the ingress of chloride and the corrosion rate of rebar at different depths. A laboratory benchmark test and a pilot-scale test were conducted to assess the performance of the system. The general and maximum localized corrosion rates, as measured by the Multi-electrode Array Sensor (MAS) probe, were all sensitive to the incremental chloride concentration in a simulated pore solution. The increasing corrosion rates were consistent with the results achieved from the standard linear polarization resistance (LPR) technique and occurred as a function of depassivation. A chloride concentration vs. potential calibration curve was established and indicated good linearity between 0.01 mol/L and 1 mol/L. The results of the pilot-scale test indicate that the corrosion rates achieved from the MAS probe varied as a result of changes in the environment and chloride concentration. Subsequently, several modifications were made to the system in order to improve field implementation: changing sampling frequency, addition of a temperature sensor, provision for temperature compensation for chloride calibration curves, and modifying the system firmware to provide current data from individual pins on the MAS sensor. A detailed guideline along with video documentation were developed as a reference to guide field implementation. This study further developed algorithms for quality control and interpretation of the sensor data. Nonetheless, a few months of field deployment of the system in an ODOT bridge pier revealed its weaknesses and additional studies are recommended to improve the robustness and long-term performance of such a system when exposed to aggressive field environments.

In the laboratory, custom-made chloride probes along with the SwRI sensor, a conventional Ag/AgCl probe (as control), and three rust-free, bare steel #4 rebars went through a cyclic immersion in the simulated concrete pore solutions. For the 9-pin MAS, the following parameter, *standard deviation of maximum ΔE/ average of average ΔE* exhibited a very strong correlation with the chloride concentration of the simulated pore solutions. For the 6-pin MAS, the following parameter, *maximum of maximum ΔE/ average of average ΔE* exhibited a very strong correlation with the chloride concentration of the simulated pore solutions, whereas the *standard deviation of maximum ΔE/ average of average ΔE* exhibited a very strong correlation with the average corrosion rate of carbon steel rebars. This demonstrates the great potential of using the 6-pin MAS as a reliable tool to predict the rebar corrosion rate even in the case of active corrosion and high chloride concentration, which warrant additional research.

Only one of the three SwRI Ag/AgCl probes was found to be a reliable chloride probe after the eight cycles of weathering. This highlighted the need for further improving the approach to fabricate the Ag/AgCl probes to serve as chloride probes in concrete. Meanwhile, three WTI custom-made chloride probes (with the appropriate treatment by proprietary coating) showed great promise in this regard. Only one of the three SwRI graphite probes remained relatively stable over the eight cycles of weathering, with its potential showing a standard deviation of 11 mV and a COV of -6%. Interestingly, a few of the WTI custom-made Ag/AgCl probes showed

good potential to serve as reliable reference electrodes in concrete. The vast majority of the sensing probes featured a response time of less than 60 seconds.

The field demonstration of a corrosion sensing system using the SwRI sensor in the Oregon marine environment revealed key challenges to be addressed in future research, including the need for more weather-proof power supply and electronics as well as better chloride sensors integrated with moisture and temperature sensors.

SUGGESTED RESEARCH

- Future research should focus on integration of miniature moisture and temperature probes, enhancing the sensor longevity inside the field concrete, and improving the system reliability, usability and cost-effectiveness.

- Additional research should validate the use of parameters from the 6-pin MAS probes, such as *maximum of maximum ΔE/ average of average ΔE*, *standard deviation of maximum ΔE/ average of average ΔE*, or other index calculated from the MAS probe readings (e.g., localized index using the software of *electrochemical noise analysis*) to reliably estimate the chloride concentration and rebar corrosion rate even in the case of active corrosion and high chloride concentration.

TABLE OF CONTENTS

LIST OF TABLES

LIST OF FIGURES

1.0 INTRODUCTION AND RESEARCH APPROACH

1.1 PROBLEM STATEMENT

Reinforcement corrosion induced by chloride contamination is a leading cause of structural damage and premature degradation in reinforced concrete (RC) structures. Approximately 90,000 bridges built in the United States are classified structurally deficient and/or functionally obsolete, representing approximately 15% of the total number of bridges in the country. Remediation projects for concrete bridges undertaken as a direct result of chloride-induced rebar corrosion was estimated to cost U.S. highway departments $5 billion per year, aside from the safety and reliability implications. Concern is the greatest in coastal and northern states where these structures are exposed to marine environments and deicing salts, respectively, such as in the state of Oregon. The Oregon Department of Transportation (ODOT) has historic RC bridges along the Pacific coast that experience serious corrosion and degradation. Like other DOTs, ODOT is faced with the difficult and expensive task of more frequent routine corrosion inspection of aging infrastructure to enhance on-time maintenance decision making.

Currently, ODOT conducts labor-intensive corrosion surveys of its coastal bridges to determine the timing and type of remedial action they require. For instance, Figure 1.1 shows a typical corrosion damage pattern for ODOT coastal bridges. Consequently, ODOT tends to focus on obtaining chloride content profiles and rebar corrosion status on the side of the girder near the bottom where corrosion damage is most likely. A method of obtaining frequent corrosion information would provide better condition assessment at much lower cost than the periodic hands-on surveys.

Figure 1.1: Two photos of the same reinforced concrete girder showing no concrete damage on the ocean-facing side (left) and corrosion damage on the face of the beam opposite the ocean (right).

Current ODOT practice generally involves concrete coring at four select locations on each bridge. At each location, three cores are obtained for enhanced data reliability. Thereafter, each obtained concrete core is assessed in the laboratory for its chloride content at every 1/2″ of depth down to 2″. If successful, the corrosion sensors would be deployed in place of concrete coring

and follow such configuration to achieve a systematic understanding of the corrosion condition for an entire ODOT RC structure.

1.2 PROBLEM BACKGROUND

The inherent drawbacks of available corrosion sensors are their inability to effectively monitor the overall evolution of corrosion in RC structures and to detect or quantify the corrosion risk prior to corrosion initiation. Currently available commercial or laboratory prototype sensors for rebar corrosion are typically placed in new structures during casting and, thus, are not suitable for corrosion sensing of existing RC structures. Arguably, corrosion sensors are most needed for existing structures that have endured decades of environmental exposure conditions (e.g., high humidity/wetness and chloride contents) and are faced with an *imminent* risk of rebar corrosion and concrete cracking. All currently available sensors have their limitations. For example, some are too large to be embedded in existing structures or they have an insufficient number of sensor types to illustrate the full picture of the rebar–concrete interfacial environment and associated corrosion risk. The longevity and reliability of these sensors are questionable inside concrete over extended periods within aggressive environments. Furthermore, corrosion damage inside concrete is difficult to detect particularly at the initiation stage.

A significant challenge for infrastructure managers and maintenance personnel is the ability to analyze sensor data and make informed maintenance decisions. The use of real-time data for corrosion diagnosis and prognosis is still relatively unexplored and the ability to intelligently interrogate the multi-parameter, time-series, noise-containing sensor data is currently lacking. Embeddable sensors for on-line monitoring of multiple concrete state variables present a great opportunity for the structural health monitoring of RC structures, considering the abundance of data available for mining.

In light of the aging infrastructure and dwindling maintenance budgets, it is necessary to develop a small, reliable, embedded, multi-parameter sensor system to be deployed at distributed locations of existing RC structures that can capture the critical data indicative of chloride ingress, corrosion initiation and possibly early-age corrosion propagation. Such an effective, adaptive, field-deployable system would meet the urgent ODOT needs for corrosion monitoring, detection, and diagnosis as well as for the assessment of the remaining life of RC structures.

1.2.1 Working Technology for the Sensing System

This section briefly describes the working technology underlying each of the sensing elements in the sensing system developed by Southwest Research Institute (SwRI). For the sensor prototype, the sensing elements included a 9-pin Multielectrode Array Sensor (MAS) probe at rebar depth and chloride probes at various depths in concrete along with a reference probe. While not part of this project scope, sensing elements for other parameters such as corrosion potential (E_{corr}), temperature, pH, and moisture, could be incorporated in an advanced version, if needed. According to the discussions with the project technical advisory committee (TAC), concrete carbonation is not a big concern in Oregon; as such, the pH of solutions in concrete generally does not change significantly along the concrete depth or over time. In this project, we measured the temperature inside the concrete at the same depth, with a temperature probe separate from the integrated corrosion sensing system. While MAS or a separate sensing element could be used to

monitor the E_{corr} of simulated rebar in concrete, the sensing of E_{corr} was deemed less important than that of the corrosion rate of the simulated rebar and the chloride content depth profile in concrete. Similarly, while the moisture content in concrete is a key parameter to the corrosion risk, it was deemed to be reflected in the corrosion rate data.

A graphite rod was used as the pseudo-reference electrode in concrete as its electrochemical potential is relatively insensitive to the local contents of chloride and hydroxyl ions. A custom-made silver/silver chloride (Ag/AgCl) electrode was used as the chloride probe in concrete. An Ag/AgCl electrode is commonly used as a non-destructive tool in analytical chemistry to quantitatively determine the free chloride concentration or to continuously monitor its temporal evolution in aqueous solutions. The electrochemical potential of the chloride probe, measured against a stable reference electrode in the same environment, shows a strong linear relationship with the logarithm of the chloride activity (a_{Cl^-}). The a_{Cl^-} can be reasonably approximated as chloride concentration when the sensor is placed in concentrations with ca. 0.5 M OH^- (e.g., simulated concrete pore solutions). The Ag/AgCl electrode in cement-based materials (mortar or concrete) has been used as an embedded reference probe for cathodic protection systems, where they showed good long-term stability over several years. However, the stability of Ag/AgCl electrodes was poor at very low chloride contents. In this project, some engineering improvements were made to the custom-made Ag/AgCl electrode to improve its longevity as a chloride probe in concrete.

The Southwest Research Institute (SwRI®) patented MAS technology was used to measure the corrosivity of the local environment in concrete. Instead of directly measuring the corrosion rate of the actual rebar embedded in concrete, the MAS measures the instantaneous corrosion rate of multiple miniature electrodes (~1 mm in diameter) made of the rebar material. The use of MAS sensors is intended to capture dramatic changes in the instantaneous corrosion rate, instead of incremental changes. The MAS sensor was less than 1 cm in diameter, with 9-pin electrodes sealed in an inert epoxy matrix, similar to the patented version shown in Figure 1.2 (which however has 16-pin electrodes). The risk of crevice corrosion was eliminated through careful fabrication of the MAS sensor.

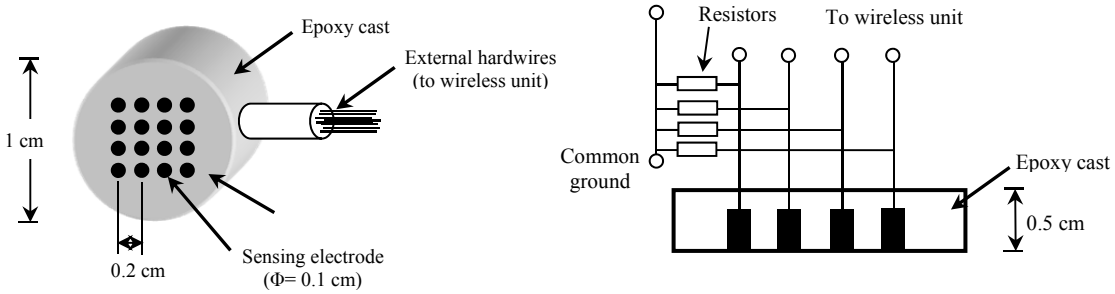

Figure 1.2: Schematic representation of a 16-pin MAS probe

The small pins are coupled together by connecting each of them to a common ground through independent resistors. The coupled MAS pins conduct corrosion current measurements by reading the differential voltage across precision 100 Ω resistors. The resistors are connected in a series chain, each connection mode being a port to an electrode of a corrosion probe array. In this manner, currents originating from an individual pin can be measured in sequence. In a corroding

environment, anodic currents flow in the more corroding pins (anodes) and the counteracting cathodic currents flow out of the less corroding pins (called cathodes). This MAS design is suitable to measure corrosion rates in non-uniform corrosion processes where the electrochemical reactions may differ on the different pins (electrodes). As a result, each pin would develop its own electrochemical potential and current. The total anodic corrosion current may be expressed as:

$$\boldsymbol{I_a = I_a^t + I_a^c} \quad \textbf{(1.1)}$$

where I_a^t is the external anodic current that flows between pins (electrodes) and I_a^c is the internal anodic current that flows from the cathodic sites within each pin (electrode). To measure I_a, the coupled MAS relies on the measurement of I_a^t. The internal current I_a^c cannot be directly measured but is small enough to be ignored for small diameter electrodes. The current density so measured is utilized as the corrosion signal since it is proportional to the corrosion rate of the metal.

1.3 STUDY OBJECTIVES

The goal of this research is to develop a reliable, cost-effective corrosion monitoring system for existing RC structures. To this end, the research objectives include: 1) improving and validating the SwRI corrosion sensor prototype for use in the concrete corrosion monitoring system; 2) developing algorithms for quality control and interpretation of the sensor data; 3) making viable recommendations to implement the corrosion monitoring system for existing DOT inventories of RC bridges; and 4) delivering a deployable prototype corrosion sensing system for DOTs to continue field evaluation.

In the project, the corrosion monitoring system included: 1) an integrated sensor that can be easily embedded into existing RC structures and *in situ* monitoring of localized chloride content profiles and corrosivity (using SwRI-patented MAS technology); 2) a web-based wireless data communication and acquisition system; and 3) a software program that interrogates the collected sensor data for quality control (QC) and corrosion risk assessment. The sensor data were automatically and periodically obtained to shed light on the risk of rebar corrosion and the health of the concrete. The overall system was designed to provide critical, actionable information and facilitate asset management and decision-making related to infrastructure maintenance and rehabilitation. Structural health prognosis, made possible by the use of multiple, miniature sensors embedded in aged structures, aimed to provide a means to analyze the current state of corrosion and possibly predict when maintenance actions would be needed.

1.4 RESEARCH APPROACH

1.4.1 Task 1: Improving Sensor System Prototype and Benchmark Testing in the Laboratory

The focus of this task was to configure the sensors for use in bridge structures and integrate the sensors with a wireless sensor platform. The SwRI sensor prototype consisted of probes for chloride concentration ($[Cl^-]$), pH, corrosion risk (MAS probe), and concrete resistivity, and a

reference probe aligned in a 1½″ × ¾″ polyacrylate cylinder mold (Figure 1.3). A ribbon connector was used to connect the individual transducers to the wireless sensor platform.

In this task, a prototype of the reconfigured corrosion sensor was fabricated and benchmark parameter calibration testing was conducted. The objectives were to:

1. Modify sensor configuration (eliminate the concrete resistivity and pH probes, extend the chloride sensing unit into a sensor array) such that the most valuable data parameters are acquired;

2. Select sensor housing materials and optimize sensor alignment to make it suitable to be embedded into both new and existing RC structures;

3. Improve the fabrication of chloride probes for better longevity in concrete;

4. Modify platform configuration to be compatible with new sensor configuration;

5. Validate the modified sensor system and calibrate its performance.

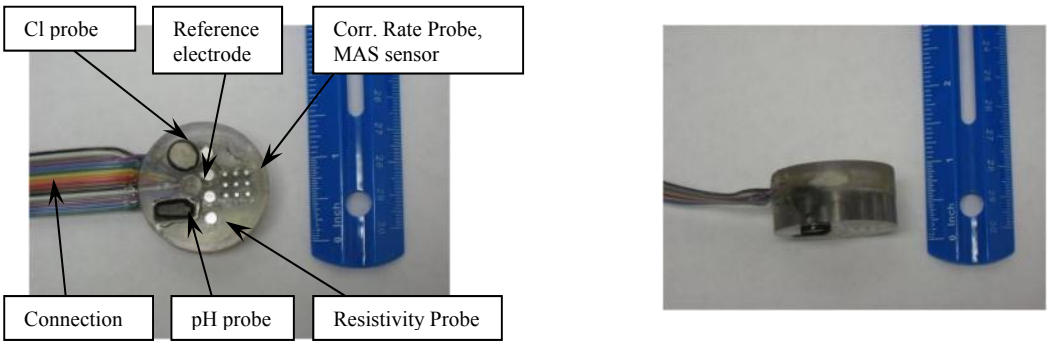

Figure 1.3: Prototype sensor configuration and profile.

1.4.2 Task 2: Testing Sensor Longevity and Validating Embedment Method.

The focus of this task was to test the longevity and reliability of the critical sensing elements in the built system and to develop and validate an embedment method that does not significantly compromise the local environment in the concrete to be monitored.

The long-term integrity and stability of the MAS probe, chloride probes and reference probes integrated into one sensor are critical to the success of this project and to the success of the sensing system for their practical application in ODOT concrete structures. As such, they were evaluated in an accelerated manner, by regulating the critical environmental variables (e.g., alkalinity, chloride concentration, heat, and moisture) during controlled "weathering tests". The weathering tests subjected the integrated sensor to a cyclic procedure of immersion in simulated concrete pore solutions (0.6M KOH + 0.2 M NaOH + 0.001 M $Ca(OH)_2$) with a given NaCl concentration for two weeks at 104ºF (40ºC) and subsequent drying by air for 3 days at room temperature. In the first four cycles, the hours of wetness had the NaCl concentration increases from 0.001 M, to 0.01 M, 0.02 M, and ultimately 0.03 M. This was followed by another four cycles, where the hours of wetness had the NaCl concentration increases from 0.04 M, to 0.06 M, 0.08 M, and ultimately 0.10 M.

During the hours of wetness, the sensing elements were connected to the data acquisition system and their readings were taken at least on an hourly basis to monitor their stability during the immersion time and as a function of wetting cycle. The sensitivity and error levels of each sensing element were analyzed as data become available.

Before and after each weathering cycle, the potentiometric response of the Ag/AgCl electrodes were measured in saturated $Ca(OH)_2$ solutions simulating the concrete pore solution contaminated by free Cl^- concentration ranging from 1×10^{-4} to 2 M to see whether they still maintained good linearity with the logarithm of the Cl^- concentrations.

Similarly, the potentiometric response of the reference probe in the sensing system were measured against that of a reference electrode that did not undergo the weathering tests. The purpose of this test was to determine whether they are prone to the exposure to various solutions, heating or wet/dry cycling.

The corrosion rate of the MAS probe were measured against that of three bare steel rebars that also underwent the weathering tests. This was to ensure that MAS results are consistent with the corrosion rate of rebar (measured via electrochemical impedance spectroscopy - EIS).

During this task, the optimal method of embedding the integrated sensor into existing RC structures was also finalized. The sensor embedment method was designed to best capture the possible two-dimensional diffusion of water and chlorides seen in ODOT bridge girders (see Figure 1.1).

1.4.3 Task 3: Demonstrating Pilot-Scale System in the Laboratory and Establishing Guidelines for Sensor Implementation at Existing RC Structures

The objective of this task was to conduct a pilot-scale test in the laboratory and establish guidelines for sensor implementation at existing RC structures. Continuous monitoring for extended periods provided valuable information regarding the reliability and durability of the sensors. This task delivered a calibrated, integrated multi-parameter sensor for further field evaluation. The laboratory testing results were used to establish guidelines for the sensor implementation at existing RC structures.

1.4.4 Task 4: Developing Methodology for Sensor Data QC and Interpretation

This task developed the method and a software program to display and interrogate the collected sensor data. The actionable corrosion condition information was presented through an intuitive interface to facilitate asset management and decision-making by ODOT personnel. A methodology was developed and refined for QC/outlier detection of each sensing element in the corrosion sensing system. The chloride concentration profile at time *t* was obtained by the three chloride probes embedded at different depth of the concrete. Such data were designed to enable the periodical evaluation of the remaining service life of the RC structure. However, due to data quality issues detailed later, such service life prediction was found to be infeasible.

1.4.5 Task 5: Demonstrating the Pilot-Scale System in the Field

This task tested and validated the performance of the overall corrosion monitoring system (including both hardware and software) in the field. The developed sensing system was deployed in an aging ODOT RC structure in the actual coastal environment. To place the sensor in the existing RC structure, a core was extracted from the chosen exposure environment. The integrated sensor was then embedded in concrete following the guideline established in Task 3. The electronics package was placed at a convenient location on the outside of the bridge column. The response of all probes within sensors were monitored every six hours and the data were downloaded and analyzed on a monthly basis.

2.0 FINDINGS

2.1 CORROSION SENSOR SYSTEM

A field deployable sensor system for monitoring chloride ingress and corrosion rate was developed. In this section, changes in the sensor configuration are addressed. Further, improvements to the original chloride probe and system fabrication are described. A description of the electronics and low-power wireless radio are provided.

2.1.1 Sensor Configuration

The corrosion sensor used in this project was based on the corrosion sensor developed and patented by SwRI®. The patented sensor unit prototype includes a multi-electrode array sensor (MAS) to be used as a corrosion current probe, an Ag/AgCl chloride probe to be used as chloride probe, a mixed metallic oxide (MMO) probe to be used as pH probe, and a four-point concrete resistance measurement probe. The sensor is capable of monitoring rebar corrosion current, chloride content, pH, and concrete resistivity *in situ*. Based on discussions with ODOT, the pH and concrete resistivity probes were removed from the original design. The rate of chloride ingress and rebar corrosion rate at various depths were critical parameters for the assessment of degradation risk and structural failure. Therefore, the built sensor body included an array of units with two or three probes implemented in each unit. The sensor used in this project, involving an array of sensor units, is shown in Figure 2.1. Both MAS and Ag/AgCl probes with a graphite reference probe were included in sensor unit 1 and 2. Only the Ag/AgCl probe and a graphite reference were included in sensor unit 3.

2.1.2 Improvements in the Chloride Probe Fabrication

Although conventional Ag/AgCl probe remains sensitive to variations in chloride content in a highly alkaline concrete environment, the insufficient service life of such a probe is a key concern with its use for long-term field applications.

The limited longevity of an Ag/AgCl probe is generally attributed to the highly alkaline concrete environment leading to the oxidation of the Ag/AgCl sensing interface. The general Ag/AgCl probe fabrication process involves dipping an Ag rod into a molten bath of AgCl to develop a thick AgCl coating as shown in Figure 2.2(a). One disadvantage for this approach is that the contact area between the Ag rod and AgCl coating is a relatively small and flat surface which may lead to the oxidation of the Ag/AgCl interface by hydroxyl ions at a relative fast rate. Based on field experience, a greater Ag and AgCl contact area or a more complex Ag/AgCl probe geometry can effectively improve longevity of the probe in high-alkalinity environments. Currently, the mechanism underlying the effectiveness of this increase in a probe surface area is unclear, but a possible explanation is that the greater contact area or complicated Ag/AgCl probe geometry increases the time required for the hydroxyl ions to oxidize the silver at the Ag/AgCl interface, thus delaying its degradation as a chloride probe.

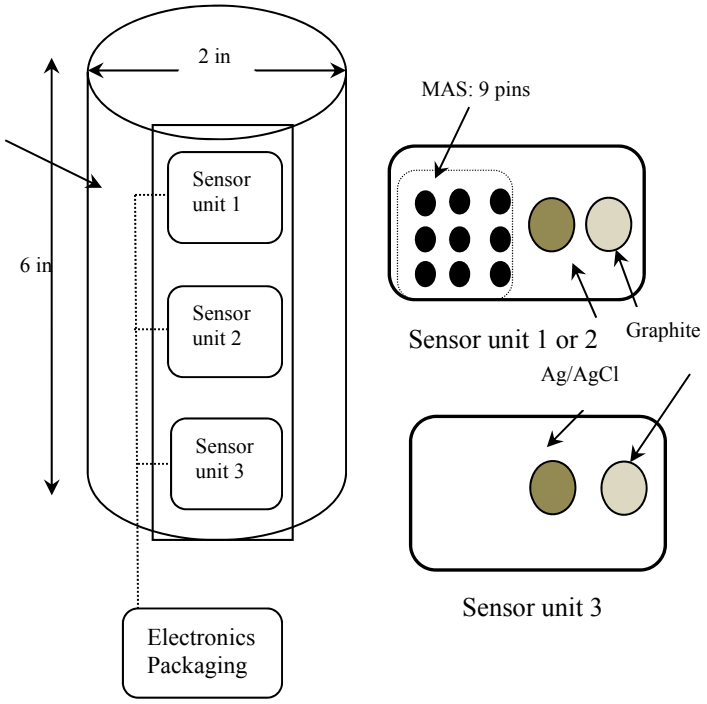

Figure 2.1:The configuration in the built sensor

(a) (b)

Figure 2.2: Ag/AgCl probe with different fabrication approaches: (a) conventional and (b) current.

In order to expand the Ag/AgCl contact area and complicate the geometry of the probe, the fabrication process was improved and is described below. After dipping the Ag rod into molten AgCl two times, a #20 Ag mesh (diameter: 0.04 in) was wrapped on the AgCl coating surface. Subsequently, an entire wrapped probe was dipped into the molten AgCl to promote a light AgCl coating on the surface of the mesh. After fabrication, the electrical connection between the Ag wire and mesh was checked. This new process can partially re-melt the AgCl

packed between the Ag mesh and rod and will result in a more compact bond between the Ag/AgCl mesh and Ag/AgCl wire with a larger contact area. For comparison, the Ag/AgCl probe fabricated using this new process is shown in Figure 2.2(b) and the probe fabricated using the existing process is shown in Figure 2.2(a). This new approach forms a good Ag/AgCl bond and is expected to provide an improvement in the stability of electrode potential (Ag/AgCl) over time.

Alternatively, experiments were conducted at the WTI's Corrosion & Sustainable Infrastructure Laboratory (CSIL) to fabricate 18 different Ag/AgCl probes by first electrodepositing AgCl onto Ag rods and then soaking the Ag/AgCl into a certain polymeric solutions for a given time. At each step of the fabrication process, an Olympus BX61 optical microscope was employed to examine the surface morphology of the prepared sensing surface, as illustrated in Figure 2.3. Once each probe was made, its potentiometric response was measured in five simulated concrete pore solutions with varying chloride concentrations. The data all showed very strong linear correlation between the open circuit potential of the probe and the logarithm of chloride concentration (with R-square no less than 0.96). An Ag/AgCl probe made with electrodeposition but not followed by dip-coating was used as a control for the probe longevity testing described in a later section.

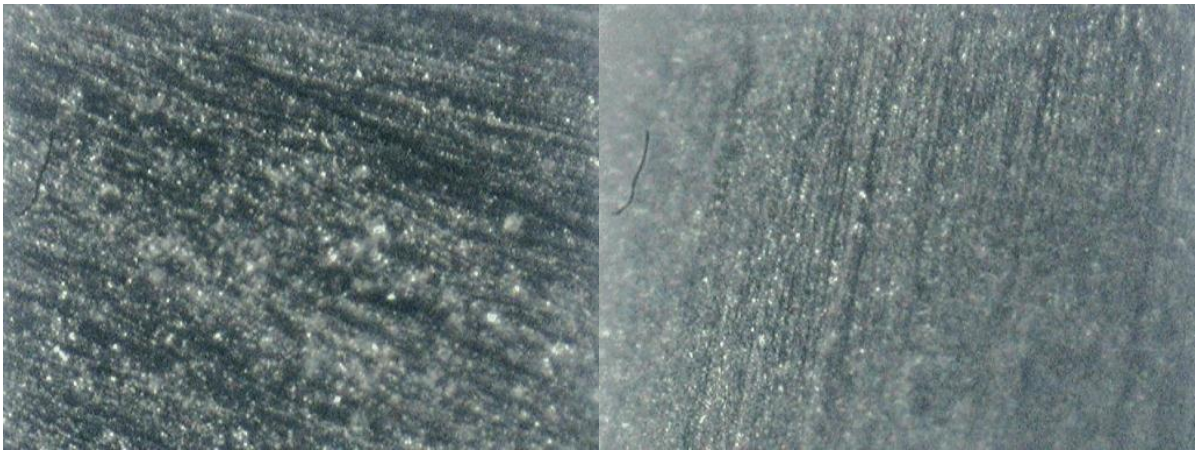

(a) (b)

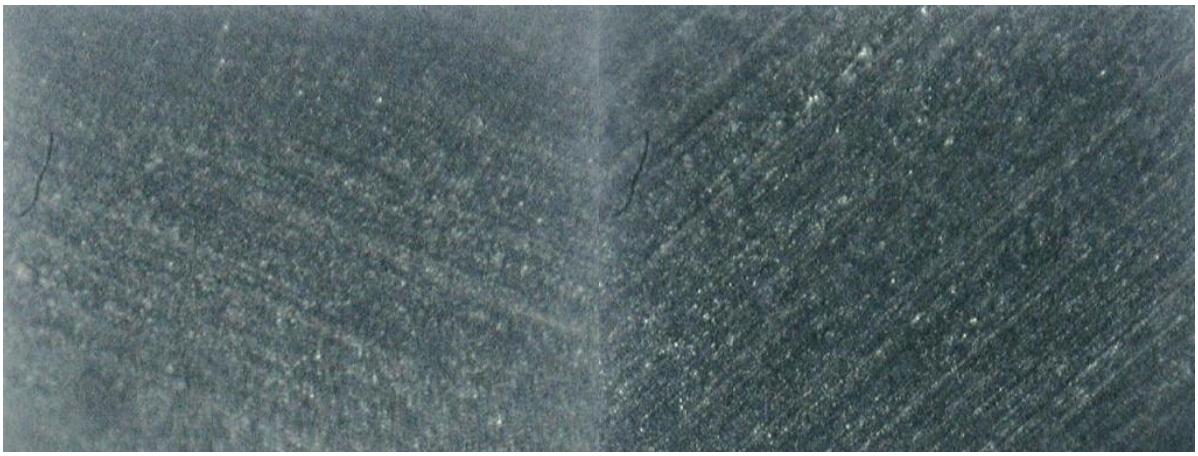

(c) (d)

Figure 2.3: Micrograph of Ag/AgCl probe surface after various stages of (a) to (c): electrodeposition and (d): polymeric coating.

2.1.3 Sensor Fabrication

Four sensor bodies were built in this project. The first two systems were built and used in the SwRI laboratory tests for probe calibration, benchmark testing and pilot-scale system demonstration and in the WTI CSIL for sensor longevity testing, respectively. The last two sensor bodies were built with minor modification based on the results of the laboratory testing. One probe was delivered to ODOT as a part of a system for field implementation. A second sensor system was fabricated for the Alaska Department of Transportation and Public Facilities. Subsequently, however, Alaska did not have a need for this sensor. SwRI personnel are continuing to search for interest in measuring concrete corrosion rate in other DOTs. For example, in Florida, there are many coastal bridges where rebar corrosion is likely. Additional DOT State agencies in the Northern Tier would be interested in this type of sensor because of the heavy use of road salts.

The fabrication process of the sensor body is described below. As schematically illustrated in Figure 2.1, polypropylene was selected as the matrix material for the sensor body. Polypropylene exhibits excellent chemical resistance in concrete structures, machinability and ease in setup of the sensor probes. A cylinder with a diameter of 2 inches and a length of 6 inches was machined. A ½ inch diameter port was hollowed out in the center from one end of the cylinder. Subsequently, the cylinder was sliced into two halves along the longitude axis such that the individual probes could be mounted internally.

The sensing probes were designed and fabricated for installation into a reinforced concrete (RC) bridge identified by ODOT. Figure 2.4(a) shows a photograph of the Ag/AgCl and graphite probes made for the sensor. A high density graphite rod was used for the graphite probe. The geometry of both the graphite and Ag/AgCl probes was ¼” in diameter with a length of ½″. An electrical wire was spot welded on the base of the Ag rod of the Ag/AgCl probe and then glued and sealed with conductive epoxy. The graphite probe was connected with a wire at the rear surface with conductive epoxy. The material used for the MAS sensing probes was a 1018 carbon steel wire with a diameter and length of 0.05 and ¼ inches, respectively. The probes were spot welded with electrical wire opposite of the sensing surface. All the probes were inserted into the designated holes after being coated with epoxy on the outer diameter surface. The coating facilitates affixing the probe in the hole and avoids humidity ingress into the electrical connection. The epoxy seal on the MAS probes avoids crevice corrosion between the probes. Epoxy was poured into the hollow tube port to seal the wire connections at the rear end of the probes. The photograph for the rear wire connection and epoxy seal is shown in Figure 2.4 (b).

The top-view photograph of the sensor prototype and the overview of the wired sensor are shown in Figure 2.4 (c) and (d). The surfaces of the MAS and graphite probes were polished to a #600 grit surface finish. The surface of the Ag/AgCl probes were indented 0.05 inch into the matrix. A 24 pin standard serial cable was used to electrically connect the MAS probes, and ribbon cables were used to connect the graphite and Ag/AgCl probes to the electrical platform. Electrical connections to all the probes were examined after assembly.

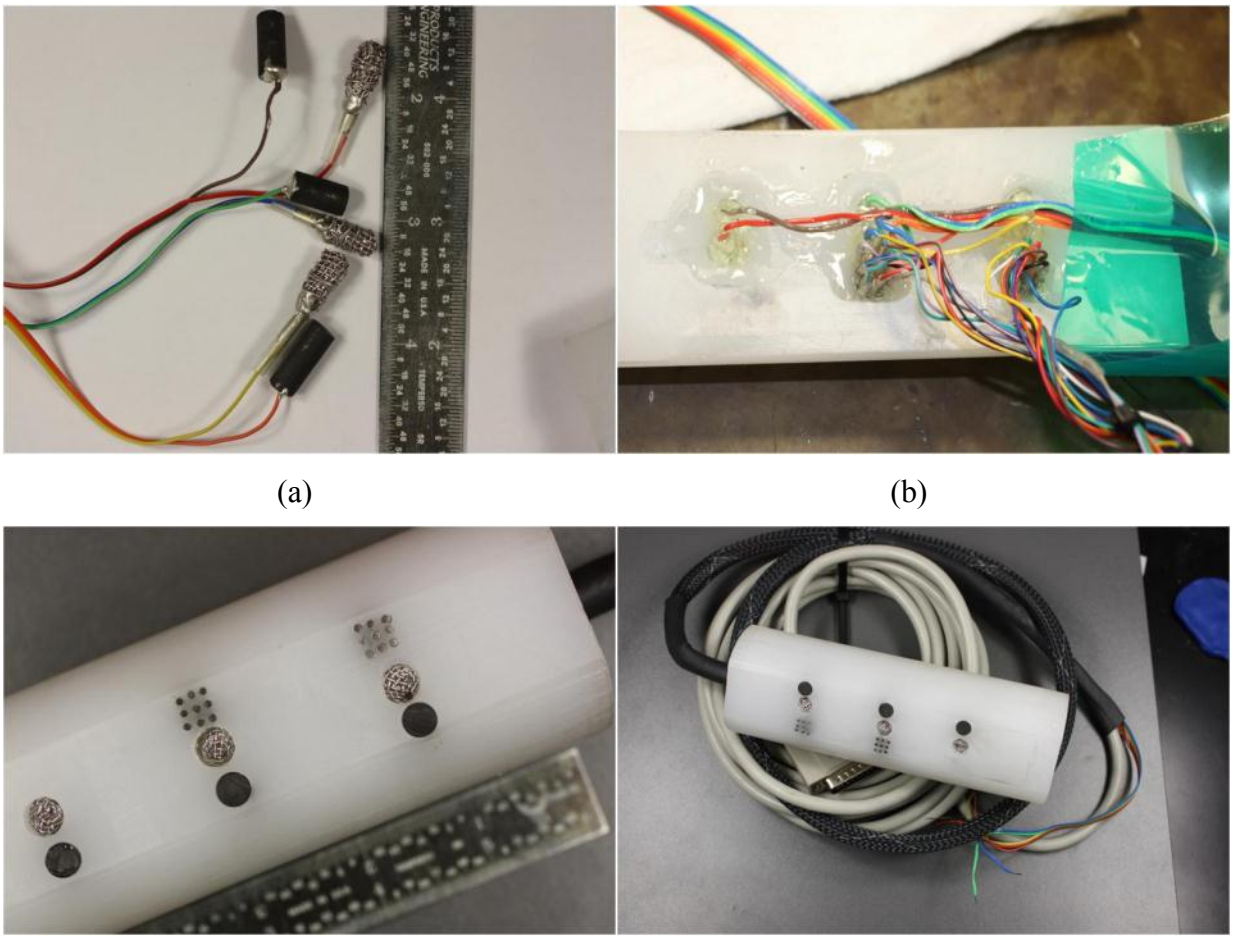

(a) (b)

(c) (d)

Figure 2.4: (a) Ag/AgCl and graphite probes, (b) wire connection inside the sensor tube, (c) top-view photograph of the sensor prototype, and (d) sensor and wired cable.

2.1.4 Sensor Electronics Platform

The sensor platform was based on a previous platform developed by SwRI and Aginova Inc. The new sensor platform and the demo sensor system are shown in Figure 2.5. In this platform, a 16-wire MAS sensor data acquisition board and communication board and two sets of electrical potential data acquisition boards and communication boards (all shown in Figure 8(a)) are included. Each board can acquire data from two Ag/AgCl probes. Therefore, one slot is left for backup purposes. Figure 2.6 is an image of the demonstration unit indicating the board address for wireless communications.

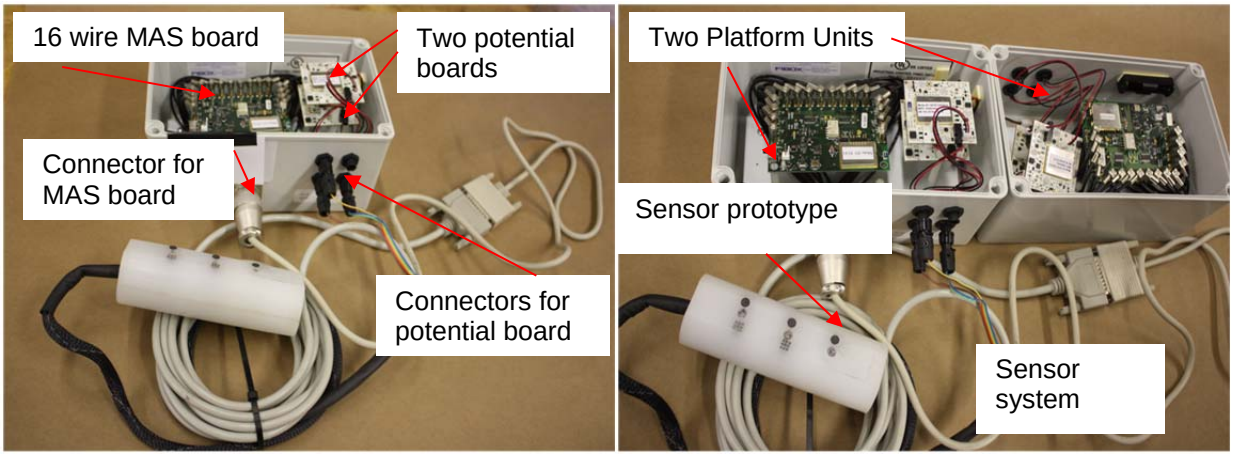

(a) (b)

Figure 2.5: Sensor data acquisition and communication platform unit

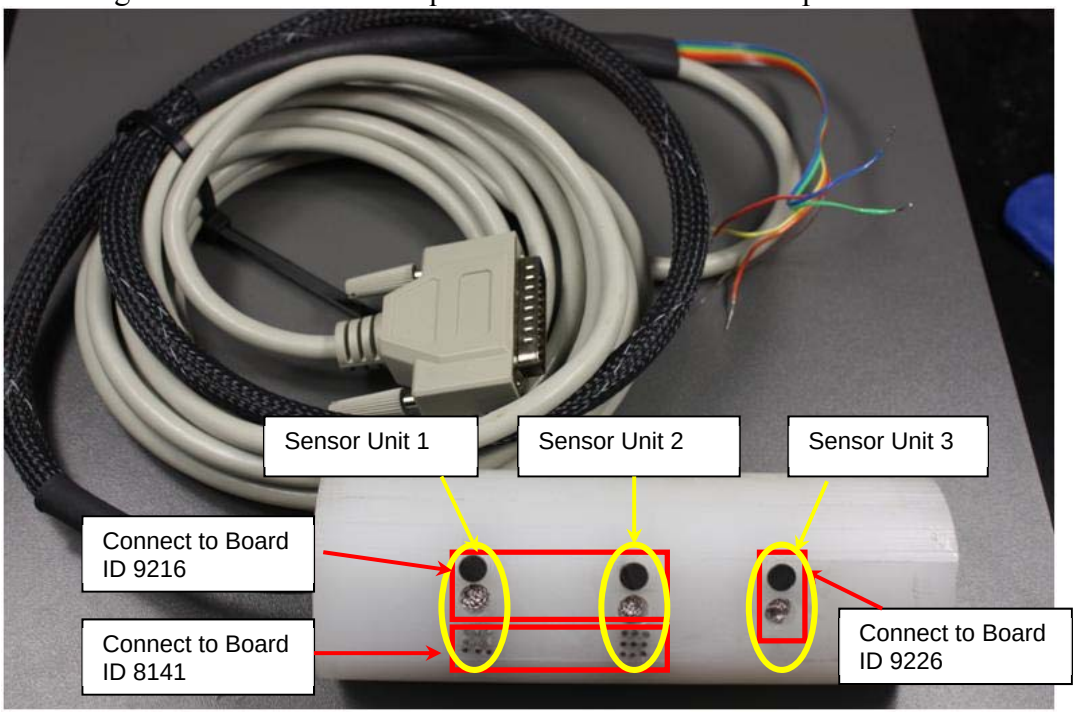

Figure 2.6:Photograph demonstration of the sensor and the connection wire.

The MAS board wire connects to the sensor through a military connector (shown in Figure 2.5(a)). In this project, the 16-wire MAS sensor board was separated into two 8-wire groups and each group connected to 8 of 9 pins in one MAS probe. The No.9 pin in both MAS probes was insulated and not connected to the MAS board. The No.9 pin may be used or kept as a backup for the 8 pins or to make a potential measurement reading in the future.

Once data is transmitted to the web portal or a PC, it can be viewed using a Graphical User Interface (GUI). The corrosion current from the 16 pins are displayed separately in a table and plot. The data from the 16 pins were manually manipulated to separate the data from the two MAS probes. Data from columns 1 to 8 represent data of pin 1 to 8 in sensor unit 1. Similarly, data from columns 9 to 16 represent data of pins 1 to 8 in sensor unit 2. Data were exported to an Excel file to calculate the average (general) and maximum corrosion current densities/corrosion rate, respectively.

2.1.5 Web-Based Wireless system and Specifications

The electronics platform uses a web-based wireless system with a low power onboard processor for continuous data acquisition. Based on the considerable amount of work on continuous monitoring for corrosion using low-powered wireless corrosion sensors, the MAS, chloride and reference probe technologies were integrated into the existing wireless sensor platform. The platform uses a low power Wi-Fi radio that transmits corrosion data through a transceiver with an ARM processor. The transceiver and detailed parameters are depicted in Figure 2.7.

An advantage of the adopted Wi-Fi based communication system is the ability to use off-the-shelf routers, thereby eliminating a significant development and implementation cost required with specialized Zigbee based systems. In the system used in this work, a commercially available NETGEAR Wireless-G Router (WGR6 14 v9)) was used. Another advantage is the use of state-of-the-art data encryption technology for security. Within the current system, a wireless gateway for sensor data collection, a web-based portal that uses web services, and a XML-RPC layer that communicates between the gateway and the portal (for storing data in databases) can be viewed using a web portal. The data acquisition unit is hermetically packaged and designed for taking measurements over a wide temperature range for up to 3 years without replacing the single 3.6 V Li AA battery. Service life was found to likely be 2 years based on short term testing.

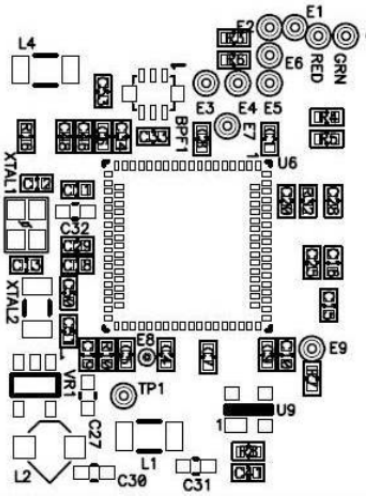

(a)

Application Processor	32-bit MCU Operating @ 44 MHz
Data Rate	Up to 2 Mbs
Radio Protocol	IEEE 802.11b/g compatible
Standards	IEEE 802.11, 802.11i,k,e,d; IEEE 1588
Security (802.11i)	WPA2, AES Encryption, EAP-FAST Authentication
I/O	GPIO, UART, 10-bit ADC

(b)

Figure 2.7: (a) Schematic for the Wi-Fi wireless transceiver with an ARM processor, (b) Specifications of the communication module

2.2 LABORATORY BENCHMARK TESTING

Testing was conducted in a representative simulated pore solution (SPS) at the SwRI laboratory. The objective of this test was to 1) calibrate the individual probes in the sensor, 2) conduct the benchmark test, and 3) evaluate the system performance. Figure 2.8 shows the detailed test setup for this calibration and benchmark testing at SwRI.

(a) (b)

Figure 2.8: Laboratory benchmark test setup (a) test cell and platform unit (b) router and laptop (software interface)

2.2.1 Test Setup

Benchmark testing was conducted in a representative simulated pore concrete solution SPS1 (pH= 13.3). Before the test, the sensor body was connected to the electronics platform, the platform was synchronized with the router, the data acquisition and GUI software was installed onto a laboratory PC and the data acquisition frequency was set to 15 minutes. At the beginning of this test, the sensor was placed in the SPS1 solution for two weeks with no chloride added. Subsequently, sodium chloride crystals were added to the solution periodically (every three to four days) to achieve specific chloride concentrations until a final concentration of 1 mol/L was reached. Data acquisition was initiated when the sensor was immersed into the SPS1 solution and ended after the chloride concentration was sustained at 1 mol/L for 10 days.

During the test, all probes within the sensor body were completely immersed in the solution, along with a conventional three electrode linear polarization resistance (LPR) test system. The system included a carbon steel rebar (#5 and 4” length), a saturated calomel electrode (SCE), and a platinum mesh counter electrode for electrochemical measurements. The three electrode system in the test solution was used to acquire the rebar corrosion rate at a certain time interval using the LPR technique. The LPR measurements were conducted immediately prior to every incremental chloride additions into the solution. The acquired rebar corrosion

rate was compared to the corrosion rate from the MAS probe at the same time to calibrate the MAS data.

Nitrogen was first purged into the solution to eliminate or minimize the effects of carbonization on the solution pH. The nitrogen purge was stopped one week later. The pH was measured periodically to record any fluctuations produced by the addition of chloride. The results indicated that pH fluctuation throughout the overall test duration was less than 0.2. The effects of this small variation of pH on potential and corrosion rate readings were negligible.

Within the test duration, three sets of data are shown on the software interface including: average corrosion rate (average of 16 pins), maximum corrosion rate (the corrosion rate of an individual pin with the most aggressive corrosion), and potential readings from three chloride sensors. Note that eight of nine pins for two MAS probes (in sensor unit 1 and 2) were connected to the MAS board (ID:8141) in the platform. Therefore, the maximum and average corrosion rate in this study represented the results of the 16 pins of two MAS probes but not the corrosion rate of one individual MAS probe. The No.9 pin in both MAS probes were insulated and not connected to the MAS transducer board. However, the sensor was immersed in the homogeneous testing solution in which the corrosion rate of the two 9-pin MAS probes should be identical. Therefore, in this calibration and benchmark test, we did not differentiate the corrosion rates of the two MAS probes.

Units 1 and 2 chloride probe readings were collected through one board (ID 9216) and the unit 3 chloride probe readings were collected through another board (ID 9226) as shown in Figure 2.6. The plots of all three sets of data can also be shown directly as a function of time in the software. The test cell and the sensor platform were setup on a laboratory bench more than 10 feet from the router and laptop in another room. The test lasted for approximately 8 weeks.

2.2.2 Test Results

In this subsection, calibration of the chloride probe and comparison of MAS data with LPR results are described.

2.2.2.1 Chloride Probes

The testing results plotted and reported in Figures 2.9 to 2.11 are the data after exporting the raw data into an EXCEL format. Figure 2.9(a), 2.10(a), and 2.11(a) show, respectively, the negative potential readings of units 1, 2, and 3 chloride probes in the sensor as a function of elapsed time and [Cl^-] concentration in the SPS1 solution. Correspondingly, Figure 2.9(b), 2.10(b), and 2.11(b) exhibit the logarithmic chloride concentration vs. the negative probe potential readings. The results in Figure 2.9(a), 2.10(a), and 2.11(a) indicate that all chloride probe potential readings are sensitive to chloride concentration variation from 0.0001 to 1.0 mol/L. The negative potential readings remain relatively stable at each specific chloride concentration and abruptly shift in the positive direction once additional chloride was added into the solution.

From Figures 2.9(a), 2.10(a), and 2.11(a), there are several anomalous observations. First, at the beginning of the test (prior to the first chloride addition), the probe potential was unstable, especially for the two chloride probes corresponding to Figure 2.10 and Figure 2.11. All probes were carefully cleaned with DI water before being immersed into the test cell. After the test, the surfaces of all chloride probes were carefully examined and no contamination or precipitation was found on the probe surfaces. The rapidly changing potential readings prior to chloride additions (Figure 2.9(a) and Figure 2.11(a)) may be attributed to the nitrogen purging and the electrochemical response time for the three probes (or the graphite reference) after being immersed in the high-alkalinity environment. This discrepancy may be minimized or totally eliminated by fabricating the probes using a consistent procedure. Under worst-case conditions, a "break in" time may be required to allow for surface stabilization prior to the acquisition of accurate measurements.

Another anomalous effect is that, for the unit 2 chloride probe (Figure 2.10(a)), the potential readings fluctuated significantly within the chloride concentration range between 0.005 and 0.05 mol/L. Interestingly, the potential readings were relatively stable before and after the chloride concentration fell in this range. This may be due to unexpected contamination, such as bubbles in the solution, forming on the probe surface and causing a "blocking" effect.

The last anomalous observation is that, at the higher chloride concentration (≥ 0.5 mol/L), the *negative* potential readings abruptly moved in a positive direction immediately after chloride addition and subsequently shifted in the negative direction. This was observed for units 1 and 3 chloride probes (shown as Figure 2.9(a) and 2.10(a)). This effect may be induced by the impact of the high and heterogeneous chloride concentration at the probe surface immediately after chloride addition. As chloride diffused evenly in the test cell, the probe potential shifted gradually towards the regular direction. It is worthy to note that the interval of each chloride addition is only three to four days, which may be too short of an exposure for a homogeneous solution to form without extra agitation, especially when high concentration of ions are added.

The anomalous observations in the preliminary calibration test helped us to further improve our probe fabrication procedure, improve our capability for data processing, and provide valuable hands-on experience for the next phase.

Figures 2.9(b), 2.10(b), and 2.11(b) show the logarithm of the chloride concentration vs. probe potential from Figures 2.9(a), 2.10(a), and 2.11(a). Note that the potential values shown in Figure 2.9(b), 2.10(b), and 2.11(b) are the average of the negative potential readings at each chloride concentration level with error bars. The error bars indicate the maximum and minimum readings taken at a given chloride concentration solution. The trend line, its linear equation, and R-square value are also indicated in the Figures. Equations (1), (2), and (3) represent the functional relationship between sensor output voltage and log of the chloride concentration of units 1, 2, and 3 chloride probes, respectively. The linear fit was performed for chloride concentration values above 0.01 M. For concentrations below this value, a threshold region begins

to appear. Note the similarity in the slope of these curves indicating relatively good reproducibility between electrodes. Because of the differences in calibration among the different sensors in simulated pore solution, calibration of each sensor must be performed prior to field deployment.

$$\mathbf{log[Cl^-] = -0.0198\ potential + 2.2323} \quad \textbf{(2.1)}$$

$$\mathbf{log[Cl^-] = -0.0147\ potential + 2.2620} \quad \textbf{(2.2)}$$

$$\mathbf{log[Cl^-] = -0.0178\ potential + 1.7632} \quad \textbf{(2.3)}$$

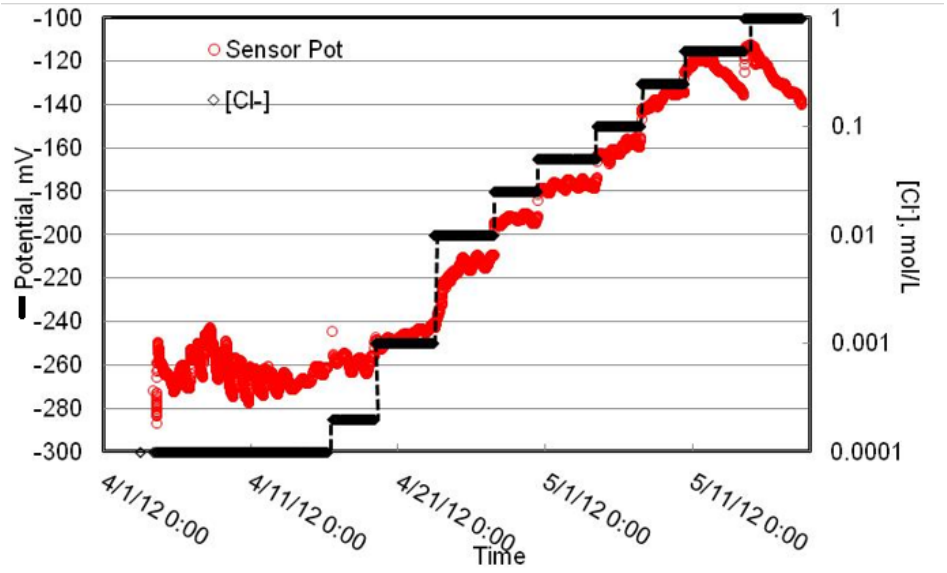

(a)

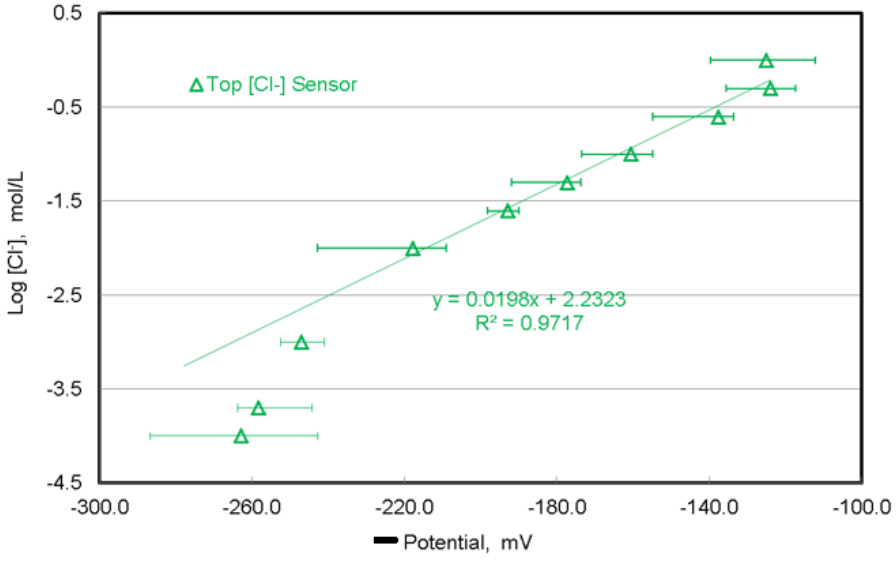

(b)

Figure 2.9: (a) Potential readings of Unit 1 chloride probe as a function of Cl^- concentration in SPS1 solution; (b) Chloride concentration vs. probe potential readings

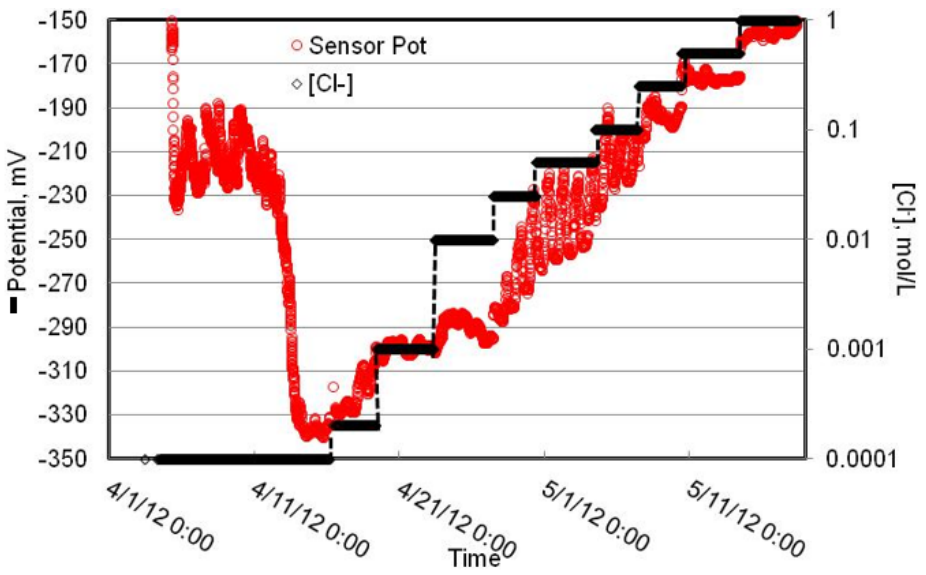

(a)

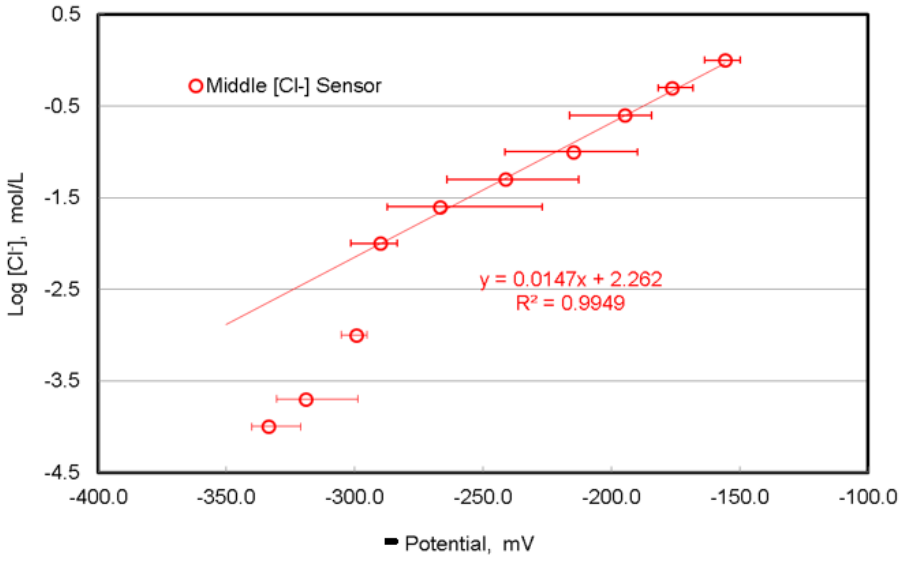

(b)

Figure 2.10: (a) Potential readings of Unit 2 chloride probe as a function of Cl^- concentration in SPS1 solution; (b) Chloride concentration vs. probe potential readings

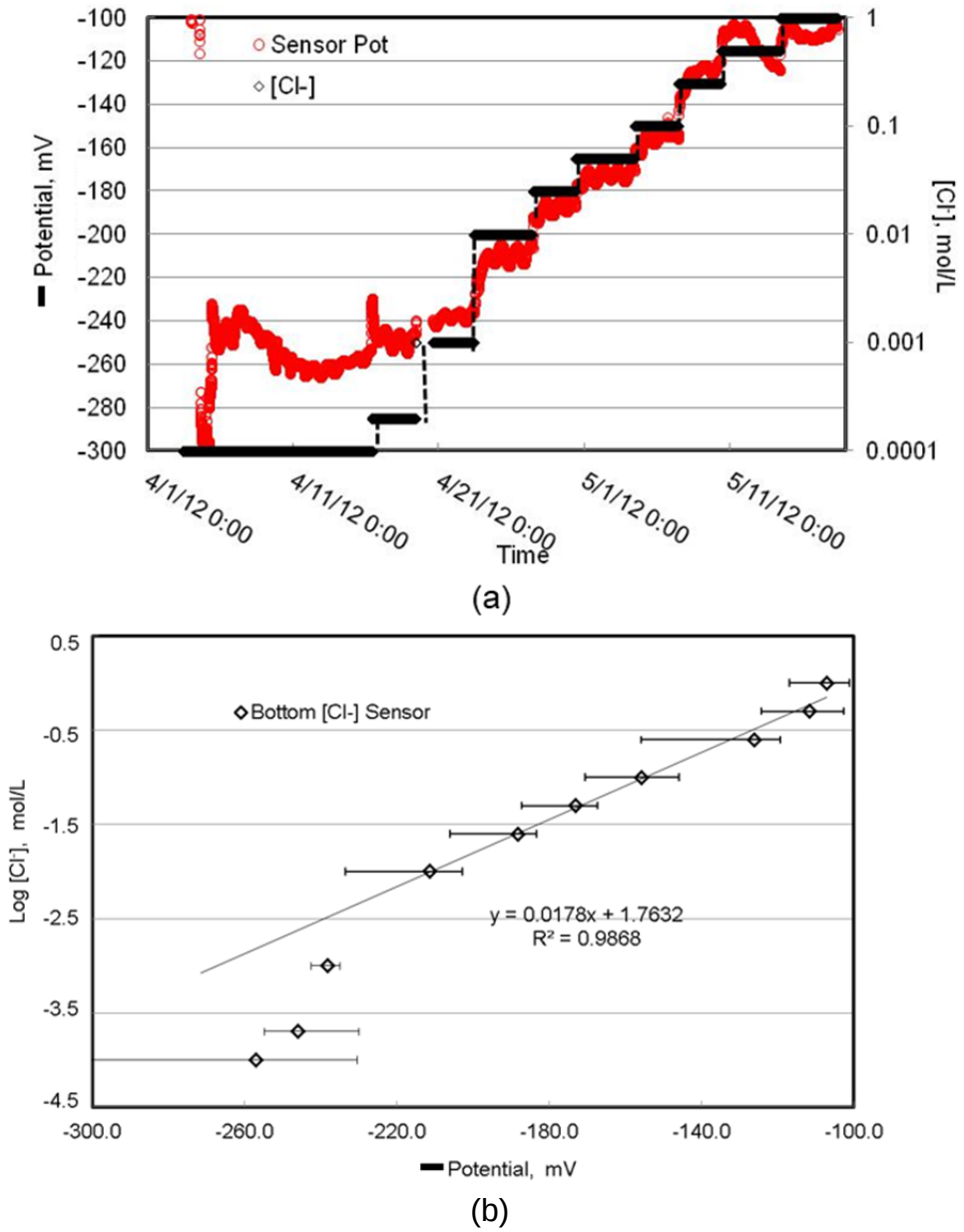

Figure 2.11: (a) Potential readings of Unit 3 chloride probe as a function of Cl^- concentration in SPS1 solution; (b) Chloride concentration vs. probe potential readings

2.2.2.2 MAS Probes

Figure 2.12 presents the results of corrosion rate for MAS and the rebar probe as a function of elapsed time and chloride concentration. Note that data were not collected during April 16, 2012 to April 20, 2012 due to a firmware problem. Fortunately, this resulted had no significant impact on the general corrosion rate trend. The results reveal that ratio of max corrosion rate to average corrosion rate provide insight into localized corrosion that occurs on steel in SPS1 solution.

For some data points, especially after April 26, 2012, parts of the maximum corrosion rate data were extremely low, shown as 0 in Figure 2.12. This was believed to be related to firmware issues with the platform. We interrupted the test and fixed the issue. Also to be noted for the data presented in Figure 2.12 is that the corrosion area of the rebar probe used in the calculation of rates was an estimate based on visual observation.

The average (general) and maximum localized corrosion rates from the MAS sensor and data from LPR measurements and calculation, increased with chloride additions. Both probes experienced passive to active corrosion transformation when the [Cl^-] was in the range of 0.020 and 0.050 mol/L. Except for a few data points ([Cl^-] at 0.025, 0.5 and 1.0 mol/L), the corrosion rates of the rebar were in reasonable agreement with the maximum corrosion rate readings of the MAS probe. This reveals that the MAS probe was a good tool to represent rebar corrosion rate in alkaline concrete environments with varying amounts of chloride present. Corrosion initiation occurred when the Cl^- concentration reached 0.05 mol/L and 0.025 mol/L for the MAS and rebar probe, respectively. Both of these two concentrations fall in the range of threshold chloride concentration to initiate rebar corrosion discussed in the literature. The cause for the discrepancy may be due to the significantly higher surface area of the rebar compared with that of the MAS probe. Statistically, greater surface exposure may induce the occurrence of localized corrosion earlier.

Another possible explanation is the short time interval (three days) for the Cl^- concentration level at 0.025 mol/L. If, as in operational environments, the Cl^- concentration changes slowly and keeps close to 0.025 mol/L for a longer duration, the MAS may activate at this chloride level. Actually, the active corrosion (abrupt increase of maximum corrosion rate) of MAS probe occurred in the second day when Cl^- level reached 0.050 mol/L. At very high Cl^- concentrations (0.5 and 1.0 mol/L), MAS and rebar probes showed a reverse corrosion rate trend. The corrosion rate of rebar increased with the increasing chloride level but the corrosion rate for MAS, both maximum and average, decreased with the increasing chloride level. This is because corrosion products adhered to the MAS pin surface which acted to suppress the corrosion rate. For the rebar probe, new corrosion spots continuously emerged on the rebar surface resulting in further corrosion processes. In other words, once active corrosion is initiated and a great amount of chloride is present, the MAS probe may no longer serve as a good tool to predict the corrosion rate of rebar unless more research is conducted to establish such prediction or correlation.

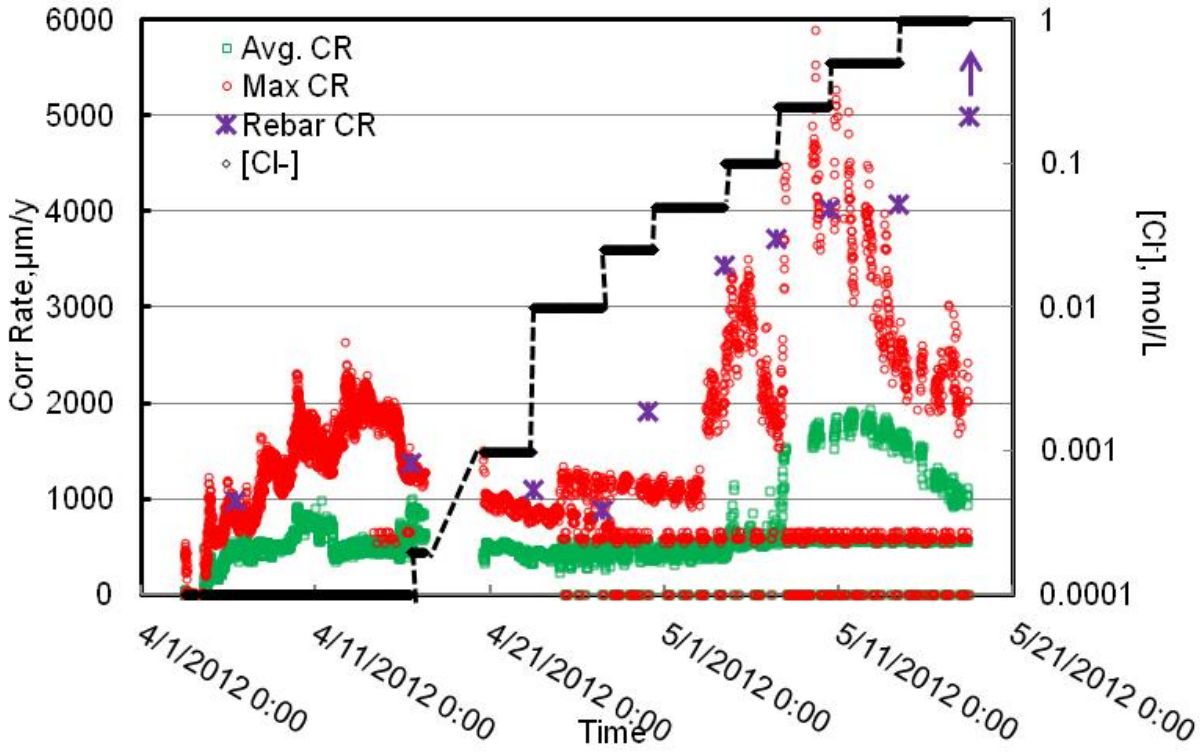

Figure 2.12: Corrosion rate, including maximum and average, results of MAS and rebar (by LPR) in SPS1 with stepwise incremental [Cl^-].

2.3 LABORATORY PILOT-SCALE TEST

The goals of this pilot-scale test were to: 1) examine the sensitivity of sensor probes to Cl- concentration variation inside a paste specimen and validate the preceding probe calibration results and 2) further evaluate the performance of the sensor system when embedded in a paste specimen. To reduce the test duration, a modified specimen configuration and test protocol were adopted for this test. The modified specimen fabrication and configuration (with probe embedded) is described below.

2.3.1 Test Setup and Procedure

Figure 2.13 photographically illustrates the specimen fabrication and curing process with consecutive pictures. The paste specimen was made of three layers with different cementitious materials and chloride concentration addition. The mix design is shown in Table 2.1. As shown in Figure 2.13(a), a stainless steel mesh (6″ diameter) was placed at the bottom of the specimen to facilitate the later application of an electric field across the fabricated specimen. In the middle and top layers, there was a well-polished rebar with a 6″ length inserted into the paste and at the same height as the corresponding probe unit.

Table 2.1:Mix Design for Pilot-Scale Test Specimen

Paste	Water/ Cement	Water, g	NaCl, g	Chloride Concentration, mol/L	Cement, g	Height in the container, in
Bottom	2/5	600	0.700	0.01	1500*	2 ½
Middle	1/3	500	2.925	0.1	1500 (Low Alkalinity)#	1 ½
Top	1/3	1050	58.50	~1.0	1500 (Low Alkalinity)#	2

*: "Alamo" type I, white Portland cement, Alamo Cement Co. (San Antonio, TX)
#:"Alamo" type I/II, low alkalinity Portland cement, Alamo Cement Co. (San Antonio, TX)

(a) (b)

(c) (d)

(e) (f)

(g) (h)

Figure 2.13: Photographic illustration of the fabrication and curing procedures for specimen with sensor embedded. (a) Positioning mold and the sensor; (b) Pouring the bottom paste layer (2 ½" thickness); (c) Preparing the middle paste layer after 24 hours of bottom paste layer pouring (with a 6" length #5 rebar inserted into the mold); (d) Pouring the middle paste layer (1 ½" thickness); (e) Preparing the top paste layer after 24 hours of bottom paste layer pouring (with a 6" length #5 rebar inserted into the mold); (f) Pouring the top paste layer (2" thickness); (g) de-mold the paste specimen after 24 hours of top paste layer pouring (a small paste cylinder of each layer paste shown was fabricated for further chloride and pH analysis); (h) Placing the specimen in a humidity chamber for 28 days curing process

The complete specimen was fabricated in three consecutive days. In the first day, the bottom paste layer was poured to a thickness of 2 ½″ with the bottom sensor set fully immersed (as shown in Figure 2.13(b)). The top and middle sensor sets were tape sealed to avoid contamination by the bottom layer paste during pouring. Subsequent to pouring, the paste was covered with plastic film and placed in an ambient temperature for 24 hours. On the second day, the plastic film was removed and a well-polished 6″ rebar segment (#5) was

inserted into the mold at the same height as the middle probe unit (as shown in Figure 2.13(c)). Next, the middle layer paste was poured to a thickness of 1 ½" submerging the middle sensor unit (as shown in Figure 2.13(d)) and the inserted rebar segment totally. Similarly, the top sensor unit was covered with tape during pouring and the paste was covered with plastic film to avoid water evaporation after pouring. On the third day, after the middle paste layer was cured for 24 hours, the plastic film was removed, a well-polished 6" rebar segment (#5) was inserted into the mold at the same height as the top probe unit (as shown in Figure 2.13(e)). The top layer paste was poured to a thickness of 2″ submerging the top sensor unit and the rebar segment totally (as shown in Figure 2.13(f)). Subsequently, a plastic film was used to cover the fresh paste for another 24 hours.

Lastly, the paste specimen was removed from the mold as a whole (as shown in Figure 2.13(g)). The specimen was placed in a warm humidity chamber to cure for 28 days. Sensor lead wires were connected to the board and the corrosion rate of the MAS probes and the potential readings of chloride probes were collected from the beginning of the curing process. Measurements continued through the end of this test. Subsequent to curing, the specimen was removed from the chamber and placed in a warm (50^0C), dry oven for around 50 days. This procedure was performed to evaporate the moisture inside the specimen.

After moisture evaporation, the specimen was removed from the oven. Several micro-cracks were visually observed on top of the specimen, which was due to the dry and warm exposure. A 6″ diameter by 4″ length of a plastic tube section was glued on to the top of the specimen as a ponding reservoir. Subsequently, 500 mL 3.5% NaCl solution was poured into the pond. The pond was covered with a plastic lid to avoid evaporation of the NaCl solution. Two days later, the NaCl solution was totally drawn into the specimen through capillary water absorption. Ponding 500 mL 3.5% NaCl solution into the reservoir was repeated three times. It took about one whole week for the solution to be totally drawn into the specimen for the third ponding, indicating that the NaCl solution penetration rate reduced significantly. In addition, there was water percolation at the bottom of specimen after the third NaCl ponding duration. These signs indicated that the chloride migration rate decreased.

To further increase the rate of chloride ingress into the specimen, an external electric field was applied to the specimen. Note that throughout the implementation of the electric field, the specimen was placed in a 1″ deep bath of saturated $Ca(OH)_2$ solution with a 2″ depth of 10% NaCl solution in the pond reservoir. The bath was to increase the electrical conductivity of the bottom part of the specimen. A piece of SS mesh (5" length by 4" width) was placed at the bottom of the ponding reservoir (as shown in Figure 2.14(a)) as a counter electrode. This SS mesh and the SS mesh embedded at the bottom of the specimen were connected to a DC power supplyr to provide the current required for chloride ingress into the specimen from the top to the bottom. A constant current (0.1mA) was applied through the SS meshes for three days. Subsequently, the current was stepped up and held at 0.2, 0.5, 1.0 mA for 3 or 4 days in each step.

(a)

(b)

Figure 2.14: Photographic illustration of the pilot-scale test at SwRI (a) close-up picture for the ponding reservoir; (b) setup for electrical injection of chloride into the specimen (0.5 A DC current applied)

2.3.2 Results and Discussion

Figure 2.15 presents the plots of corrosion rates, including general (average) and maximum localized corrosion, as a function of time. Although certain data shown in the plots were anomalous, the results still provided valuable information for further investigations.

The data were collected beginning on June 29, 2012 (also the beginning of the specimen curing process) and ended on November 20, 2012. Data from October 15, 2012 to October 30, 2012 were lost because the MAS board battery was dead. The service life of the battery in this test was short because it had been used for five and a half months for both benchmark and pilot-scale tests with a 15-minute data acquisition frequency. For field use, the data acquisition frequency should be set for 6 hours, which will provide an expected service life for the battery of more than three years.

Data for MAS probes should be separated into two groups. The data collected from pins 1~8 represent the results of MAS probe in unit 1 and data collected from pins 9~16 represent the results of the MAS probe in unit 2. However, during the test, the firmware embedded in the

MAS board did not separate the data into two groups but treated the data from all 16 pins as one group. Further, current data from individual pins were not recorded. Therefore, the general corrosion and maximum localized corrosion rates represent the calculated average and maximum values of all 16 pins. The firmware was upgraded after the test and this issue was resolved. The general and maximum corrosion rates of each 8-pin probe can be calculated manually after exporting the data to an Excel format.

Regardless of the issues of the firmware, the results of general and maximum corrosion rates from all 16-pins offer useful information to evaluate sensor function. In the curing process, from June 28, 2012 to July 25, 2012, the MAS probe experienced a severe corrosion attack. The general corrosion rates fluctuated in the range of 700 and 1200 μm/y and the max localized corrosion rates varied between 1000 and 6000 μm/y. The high corrosion rate were the results of (1) chloride pre-mixed in the paste prevented the formation of a protective passive film on the probe surface; (2) the warm (~50°C) and wet (90% humidity) environmental condition facilitated wetting of the concrete and sustaining corrosion reactions.

After curing, the specimen was placed in a warm (50^0C), dry oven from July 25, 2012 to September 13, 2012. Water within the specimen was reduced through capillary processes and the corrosion rates, both general and maximum localized dropped to a lower level as shown in Figure 2.15(a).

Figure 2.15(b) shows an expanded plot of Figure 2.15(a) from September 19, 2012 to November 20, 2012. During this period, a DC current was applied to the specimen through an external electrical field in an incremental manner. The general corrosion rates were in the range of 200 and 500 μm/y. The rates showed a relatively stable trend before the applied current reached 1.0 mA, indicating that the effects of lower applied current on chloride migration was not significant. When the applied current reached 1.0 mA, the general corrosion rates increased. Similar trends were seen for the maximum localized corrosion rate as a function of applied current. The results indicated that the greater applied current was needed to induce chloride migration inside the specimen. The variation of corrosion rates throughout the whole test duration revealed that the MAS probe was sensitive to changes in local chloride concentrations in the paste specimen.

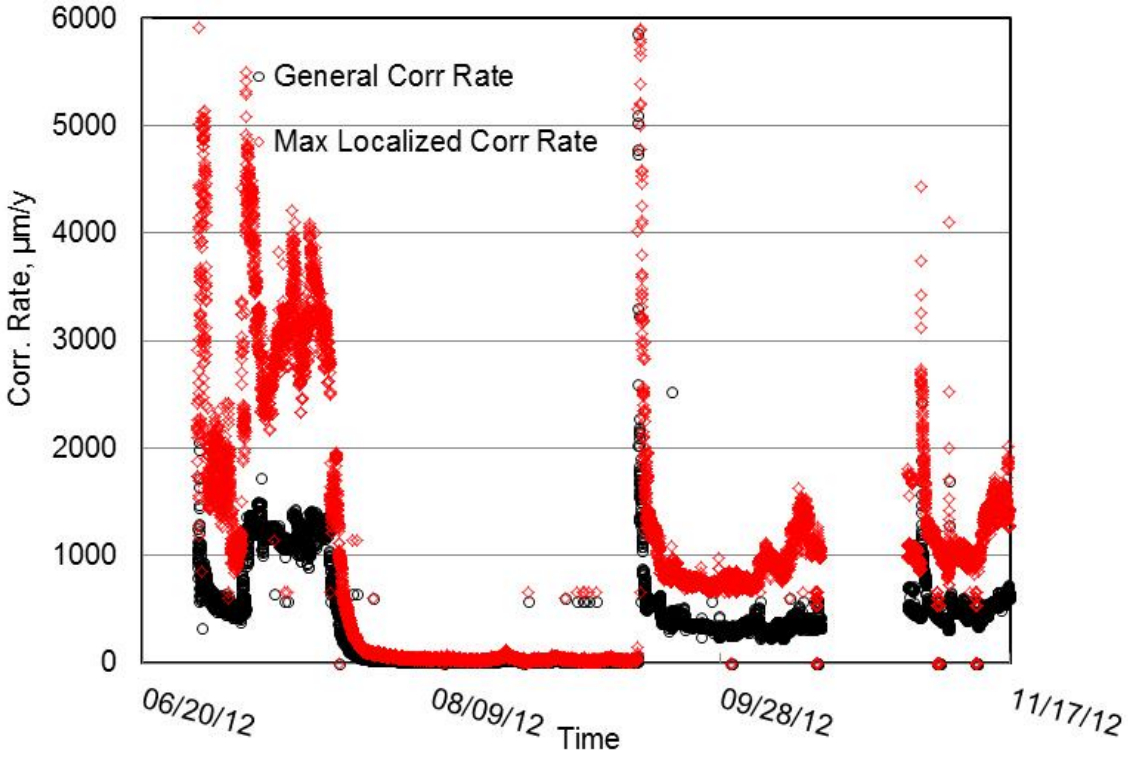
6000
5000
4000
3000
2000
1000
0
Corr. Rate, µm/y
General Corr Rate
Max Localized Corr Rate
06/20/12
08/09/12
09/28/12
11/17/12
Time

(a)

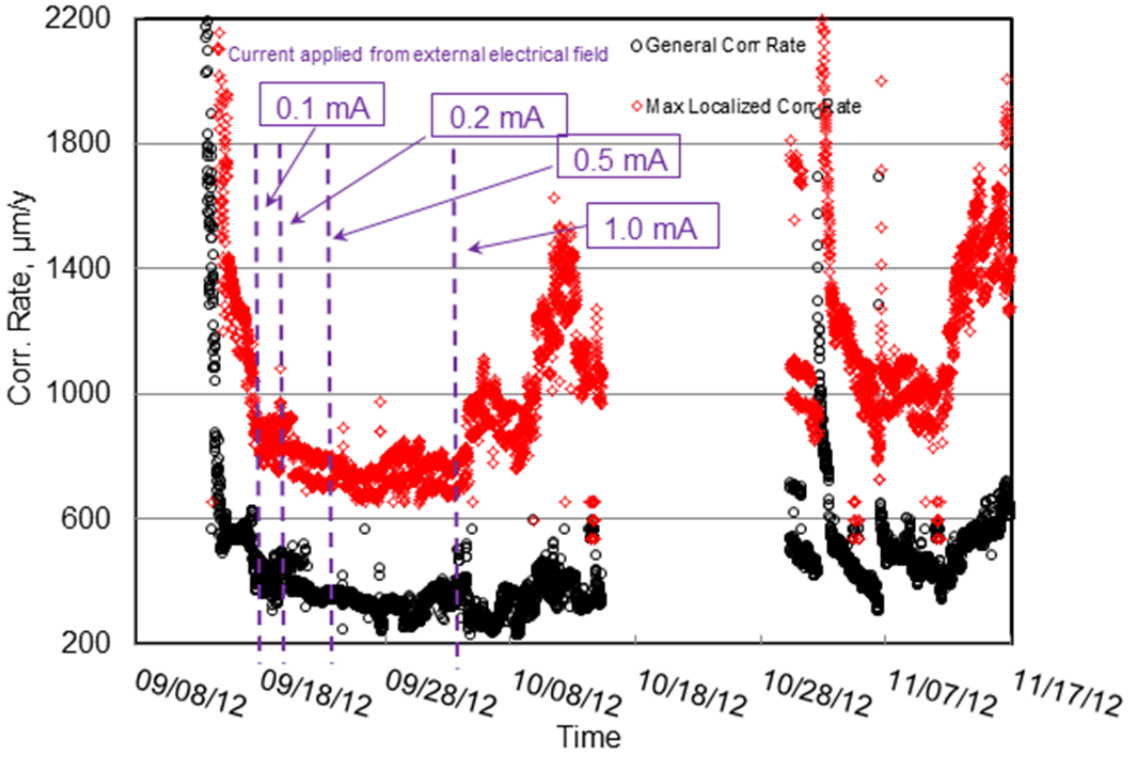
2200
1800
1400
1000
600
200
Corr. Rate, µm/y
Current applied from external electrical field
General Corr Rate
Max Localized Corr Rate
0.1 mA
0.2 mA
0.5 mA
1.0 mA
09/08/12
09/18/12
09/28/12
10/08/12
10/18/12
10/28/12
11/07/12
11/17/12
Time

(b)

Figure 2.15: Plots of general and maximum localized corrosion rates, as function of time (a) throughout the test duration and (b) an expanded plot of 14(a) from 9/19/2012 to 11/20/2012

Figure 2.16 presents the potential readings of the three chloride probes embedded in the sensor as a function of time. Prior to electromigration, the highest concentration of chloride existed in the top layer of the concrete as would be expected from the mix ratios outlined in Table 2.1 (1.0 mol/L and 0.1 mol/L for the top and middle layers, respectively). Before Sept. 28, 2012 (when the externally applied current was increased to 1.0 mA), the potential readings from the top and middle chloride probes (vs. graphite) were at approximately +145 and +101 mV, respectively. According to Equations (2.1) and (2.2), the calculated chloride contents were 0.23 mol/L and 5.99 mol/L, respectively. The calculated chloride concentration from the top layer was substantially less than the original chloride concentration prior to curing (1.0 mol/L). Chloride concentration in the middle layer greatly exceeded the pre-cured concrete (0.1 mol/L). A note of caution is that the chloride probes might have deviated from the linear relationships shown in Equations (2.1) and (2.2).

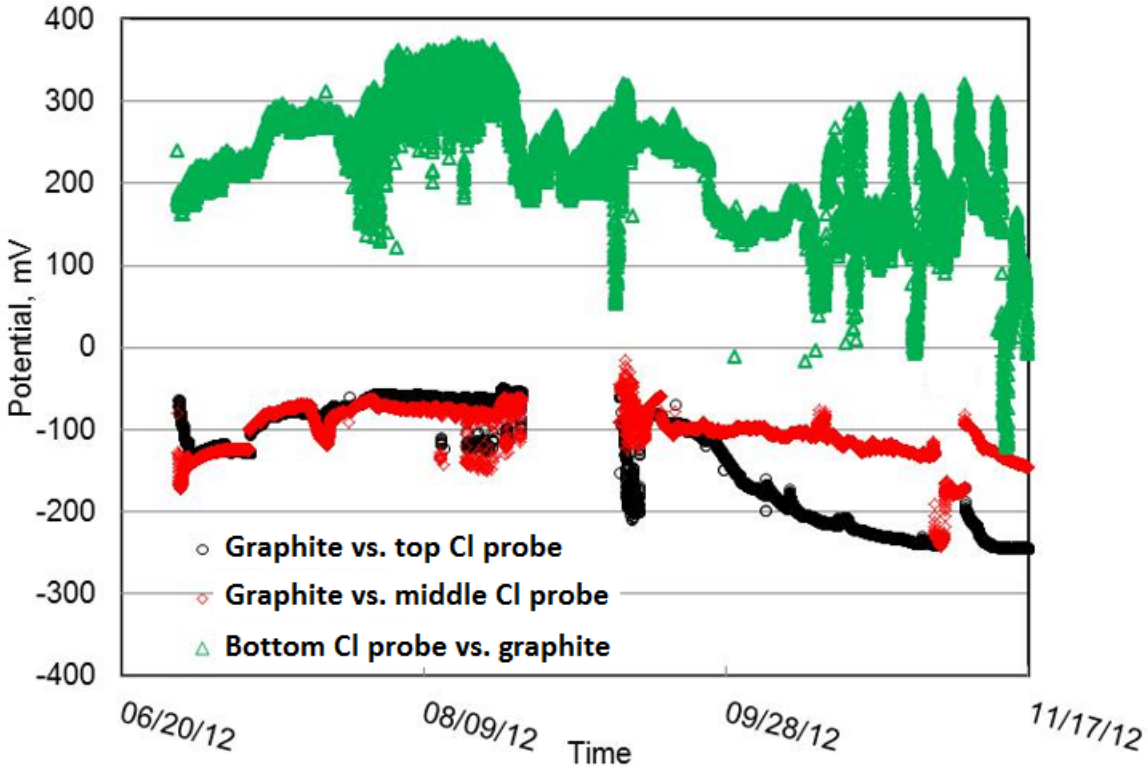

Figure 2.16: Plots of potential of Ag/AgCl probes as a function of time. For better legibility of the data, the top and bottom probes show their negative potential.

After Sept. 28, 2012 (when the externally applied current was increased to 1.0 mA), the potential readings from the top chloride probe (indicated by the block dots) shifted towards more positive direction, corresponding to a significant decrease of the chloride concentration in the top layer as a result of electromigration. Examination of Figure 2.16 indicates a rapid depletion in the chloride concentration to a value of 0.002 mol/L in the top layer of concrete.

In the middle layer, the chloride concentration also decreased as a result of electromigration, but to a lesser degree (to 1.89 mol/L).

The potential data of the bottom chloride probe (in the bottom layer of the concrete cylinder) in Figure 2.16 is unstable and varies abruptly throughout the test duration. This is mainly due to the absence of sufficient moisture and sufficient chloride ions (0.01 mol/L admixed into the fresh paste). In this case, the oxidation of the AgCl sensing layer by hydroxyl ions might be severe, which led to occasionally very low potential readings of the chloride probe. By November 2012, the probe should be reporting a potential around +150 mV, which corresponds to the [Cl-] of 0.12 mol/L according to Equation (2.3). Due to the sensor oxidation, however, the bottom chloride probe reported lower or even negative values.

Three main factors might have contributed to the significant change in the chloride probe readings during the curing process (between 7/1/2012 and 9/28/2012). First, during curing, free chlorides in the fresh cement paste can participate in the cement hydration process and become chemically bound, which would substantially decrease the amount of free chlorides in the pore solution and lead to more positive potential readings. Another potential reason may be thermal oxidation that occurred during curing at 50oC. The formation of an oxide film on the sensor surface would result in a decrease in the probes' potential. Finally, the electrochemical potential of the chloride probes would slightly decrease as a result of increasing temperature, according to the Nernst's Equation. This highlights the need for a temperature compensation factor when converting the probe potential readings into chloride concentration results.

2.4 SUMMARY AND CONCLUSIONS FOR THE SwRI LABORATORY TESTS

Based on technology developed at SwRI, a sensor probe was fabricated that can be installed on a concrete bridge structure. This probe consisted of three sensor units designed to be at different depths. Each sensor unit contained an Ag/AgCl probe and a graphite reference probe to measure chloride concentration. In addition, two units also contained multi-electrode array sensors (MAS) to measure corrosion rate. An improved fabrication procedure for the Ag/AgCl electrode was developed to help enhance the life of this electrode in the highly alkaline environment found in concrete.

The sensor was exposed to simulated concrete pore solutions with varying amounts of chloride. A calibration curve was generated that defined the linear relationship between the log of the chloride concentration and a measured potential. Similar calibration curves were shown for the 3 sensor units that were fabricated. In general, an increase in the voltage measurement error was observed for chloride concentrations below 0.001 mol/L. This value can be used as a practical threshold value.

The MAS sensor was tested against a traditional LPR sensor. The advantage of the MAS sensor is that corrosion is measured at the rest potential (i.e. no polarization), which will reduce battery consumption. It was shown that LPR and MAS data reports similar trends and values when exposed to the simulated pore solution with varying amounts of chloride. In particular, depassivation of the steel electrodes occurred between 0.025 mol/L and 0.050

mol/L chloride, which is in agreement with literature values. This was significant in that the MAS probe was able to detect the initiation of corrosion. Note that both of these values were higher than the threshold chloride concentration for the sensor. Also of importance was the similarity in the corrosion rate as measured by the MAS and LPR techniques. Slight differences in the critical chloride concentration for depassivation and measured rates at the highest chloride content were likely the result of the much larger surface area of the LPR probes.

A laboratory pilot study was performed to evaluate sensor performance under simulated field conditions. A concrete cylinder containing three layers of concrete with differing chloride content was fabricated with the sensor inside. One chloride sensor either failed or was in a region that was too dry for the sensor to function properly. The other two sensors were able to distinguish differences in chloride concentration prior to curing. Further, the sensor indicated falling chloride concentration within the top layer of the concrete cylinder after inducing chloride ion migration towards the bottom of the cylinder as would be expected. Additionally, the corrosion rate was observed to increase as chloride migrated through the concrete cylinder once the applied current was > 1 mA. Close examination of Figures 2.15 and 2.16 revealed that the increase in corrosion rate occurred at the same time that chloride depletion begins to occur in the top layer. It should be noted that the corrosion data were partially from the MAS sensor in unit 1 and partly from unit 2. Thus it was impossible to resolve the exact nature of corrosion and chloride migration. It is also thought that temperature effects played a strong role in the chloride sensor output.

Based on data collected during the pilot test, improvements can be made to the concrete sensor probe. Some of the changes are outlined below:

- Calibration curves at differing temperatures must be acquired to provide temperature compensation for measurements of chloride content.
- The firmware was upgraded for the new field deployed sensor systems in order to ensure that data from each MAS probe pin was individually recorded. This is critical to determine the depth where corrosion is occurring.
- Improvements in the probe fabrication will need to be made to accommodate rough handling that may result in mechanical damage to the probes (e.g. the Ag/AgCl probes on unit 3 and loose batteries in the electronics package).
- Measurements taken every 6 hours will ensure a battery life of over 3 years.
- A temperature probe was added to the measurement system to provide relevant information temperature compensation.

2.5 ACCELERATED TESTING OF SENSOR LONGEVITY

At the WTI laboratory, the custom-made chloride probes along with the SwRI sensor (as shown in Figure 2.1), a conventional Ag/AgCl probe (as control), and three rust-free, bare steel #4 rebars (immersed length: 2″) went through cyclic immersion in the simulated

concrete pore solutions. Each sensor went through an immersion cycle for a period of two weeks and drying cycle for 3 days. During each wetting cycle, the potential difference of each sensor was measured against SCE for every hour using the data acquisition system. The potentiometric response of each sensor was also measured against SCE before and after each immersion cycle to measure linearity.

As shown in Table 2.2, only six out of the eighteen WTI custom-made chloride probes (WTI Cl1a, WTI Cl1b, WTI Cl2a, WTI Cl2b, WTI Cl1c, and WTI Cl3) were considered reliable after the eight cycles of weathering (consisting of wet-dry and chloride concentration changes). The coefficients of variance (COVs) highlighted in red color indicate values higher than 20%, which was used as a cut-off value for identifying poor sensor stability in the test solution with a given chloride concentration. In other words, the reliable probe would feature stable potential readings during each cycle, which would translate to a COV value of no more than 20%.

As shown in Table 2.3, the control Cl^- probe (Ag/AgCl via electrodeposition only) failed to remain reliable after cycle 4, likely due to the degradation of the AgCl surface layer by the alkaline oxidation and wet-dry cycling. Two of three SwRI chloride probes remained reliable after the eight weathering cycles, whereas the 2nd SwRI chloride probe failed to remain reliable after cycle 6. All three SwRI graphite probes remained reliable after the eight weathering cycles. Note that after cycle 4 (Cl^- increased from 0.03M to 0.04M), the 3rd rebar exhibited great variability in its potential readings during each cycle, which is attributable to its active corrosion.

Table 2.2:Potentiometric responses of WTI custom-made Ag/AgCl probes during the weathering cycles

	Cycle 1			Cycle 2			Cycle 3			Cycle 4			Cycle 5			Cycle 6			Cycle 7			Cycle 8		
Name of the chloride sensor	*Average*	*STDEV*	*COV*	*Average*	*STDEV*	*COV*	*Average*	*STDEV*	*COV*	*Average*	*STDEV*	*COV*	*Average*	*STDEV*	*COV*	*Average*	*STDEV*	*COV*	*Average*	*STDEV*	*COV*	*Average*	*STDEV*	COV
Amberlite IRA - 400 Chloride	-722.4	323.9	-45%	-323.7	29.1	-9%	-378.9	51.1	-13%	-569.8	225.8	-40%	-896.1	129.5	-14%	-1001.2	239.3	-24%	-1033.1	79.0	-8%	-895.9	52.4	-6%
Polyethylene Oxide	-310.1	18.4	-6%	-328.1	17.8	-5%	-331.9	37.0	-11%	-342.1	30.1	-9%	-365.2	113.4	-31%	-356.5	36.9	-10%	-314.3	56.0	-18%	-376.7	70.4	-19%
WTI Cl1a	-159.2	8.0	-5%	-170.0	6.3	-4%	-156.7	13.3	-8%	-155.5	9.3	-6%	-170.0	5.6	-3%	-171.1	10.5	-6%	-157.3	7.2	-5%	-178.3	6.7	-4%
Polytetrafluroethylene	-416.1	70.5	-17%	-409.1	99.8	-24%	-411.7	76.9	-19%	-484.4	163.8	-34%	-973.2	118.3	-12%	-951.1	59.3	-6%	-876.2	81.8	-9%	-914.7	103.4	-11%
Poly Vinyl alcohol	-721.8	305.3	-42%	-763.0	334.3	-44%	-679.8	283.1	-42%	-649.7	303.7	-47%	-934.3	275.5	-29%									
Dextrose (Glucose) Anhyrdous	-378.4	40.9	-11%	-426.7	156.4	-37%	-499.2	217.4	-44%	-454.7	190.4	-42%	-924.6	95.3	-10%									
WTI Cl1b	-158.1	9.4	-6%	-172.4	9.2	-5%	-171.2	5.7	-3%	-167.9	7.0	-4%	-185.8	5.9	-3%	-207.6	9.7	-5%	-220.4	18.0	-8%	-252.7	12.6	-5%
Chitosan	-368.1	24.8	-7%	-820.9	322.6	-39%	-1068.7	99.4	-9%	-1055.8	97.2	-9%	-1111.2	61.9	-6%	-984.9	128.8	-13%	-774.7	43.9	-6%	-925.5	118.0	-13%
WTI Cl2a	-163.1	9.2	-6%	-174.4	11.0	-6%	-180.5	4.6	-3%	-181.0	10.4	-6%	-216.9	10.9	-5%	-252.3	15.9	-6%	-271.9	33.5	-12%	-321.8	29.7	-9%
Chitosan	-352.4	18.0	-5%	-370.2	36.3	-10%	-400.6	97.7	-24%	-360.6	57.7	-16%	-567.0	291.8	-51%	-1001.7	101.4	-10%	-709.3	203.5	-29%	-861.9	127.4	-15%
Polyethylene Glycol	-305.2	15.3	-5%	-343.1	46.9	-14%	-412.7	102.8	-25%	-342.2	116.6	-34%	-874.2	183.0	-21%	-737.1	236.6	-32%	-832.3	172.1	-21%	-890.0	94.7	-11%
Chitosan	-1047.4	140.4	-13%	-1067.6	70.8	-7%	-988.6	129.3	-13%	-815.8	230.2	-28%	-992.9	127.9	-13%	-867.6	93.9	-11%	-893.0	121.9	-14%	-907.0	96.4	-11%
poly Vinyl Alcohol	-344.9	30.3	-9%	-369.6	61.7	-17%	-477.7	193.5	-41%	-511.9	226.5	-44%	-1022.8	121.8	-12%									
Poly Acrylic acid	-354.4	21.5	-6%	-399.8	56.5	-14%	-467.4	132.6	-28%	-502.3	219.4	-44%	-1094.1	131.9	-12%									
Poly Vinyl Alcohol	-1036.8	157.8	-15%	-896.9	233.6	-26%	-934.8	136.2	-15%	-979.4	82.3	-8%	-1041.5	89.2	-9%	-775.0	12.7	-2%	-916.2	126.3	-14%	-1077.2	58.8	-5%
WTI Cl2b	-167.2	13.5	-8%	-179.3	7.5	-4%	-174.3	8.2	-5%	-172.0	7.2	-4%	-197.3	6.6	-3%	-220.2	9.1	-4%	-216.9	9.6	-4%	-241.9	8.3	-3%
WTI Cl1c	-266.4	13.1	-5%	-266.1	14.2	-5%	-281.9	17.3	-6%	-269.3	15.5	-6%	-287.2	16.2	-6%	-304.7	23.8	-8%	-276.9	23.9	-9%	-303.5	8.5	-3%
WTI Cl3	-330.2	30.9	-9%	-374.3	37.3	-10%	-358.8	26.3	-7%	-341.5	20.1	-6%	-370.9	26.4	-7%	-367.0	22.3	-6%	-348.2	19.7	-6%	-406.4	51.7	-13%

* The grey color indicates sensors being removed from the test due to poor linearity measured in proceeding cycles.
Note: The potential of chloride probes was measured against a SCE.

Table 2.3:Potentiometric responses of the SwRI sensing probes (and the control Cl^- probe) during the weathering cycles

	Cycle 1			Cycle 2			Cycle 3			Cycle 4			Cycle 5			Cycle 6			Cycle 7			Cycle 8		
Sensors	*Average*	*STDEV*	*COV*	*Average*	*STDEV*	*COV*	*Average*	*STDEV*	*COV*	*Average*	*STDEV*	*COV*	*Average*	*STDEV*	*COV*	*Average*	*STDEV*	*COV*	*Average*	*STDEV*	*COV*	*Average*	*STDEV*	*COV*
REBAR(1)	-161.9	18.0	-11%	-136.6	7.3	-5%	-151.9	20.3	-13%	-115.1	8.8	-8%	-118.7	7.0	-6%	-125.1	10.8	-9%	-107.9	33.3	-31%	-121.1	31.4	-26%
REBAR(2)	-155.9	10.7	-7%	-141.9	10.9	-8%	-134.9	2.4	-2%	-166.6	58.7	-35%	-131.3	26.3	-20%	-123.3	10.0	-8%	-100.0	9.7	-10%	-124.6	8.5	-7%
REBAR(3)	-184.0	42.9	-23%	-159.4	39.9	-25%	-124.1	20.7	-17%	-161.9	31.0	-19%	-116.4	767.6	-660%	-142.9	105.7	-74%	-324.9	66.7	-21%	-159.6	852.4	-534%
Control Cl	-203.8	13.1	-6%	-202.3	17.4	-9%	-188.0	16.2	-9%	-278.3	47.5	-17%	-495.8	244.7	-49%	-526.5	296.3	-56%	-297.9	40.5	-14%	-478.4	212.6	-44%
SWRI_CL(1)	282.7	3.5	1%	283.8	4.6	2%	261.0	18.5	7%	261.9	3.2	1%	259.7	5.8	2%	235.5	5.1	2%	206.2	23.1	11%	224.5	19.3	9%
SWRI_CL(2)	271.5	11.2	4%	275.4	28.8	10%	245.7	26.8	11%	227.1	31.3	14%	217.6	35.0	16%	145.7	47.7	33%	146.9	73.7	50%	126.3	49.0	39%
SWRI_CL(3)	267.1	9.1	3%	269.6	16.3	6%	261.4	14.1	5%	272.0	15.9	6%	297.6	18.3	6%	306.2	28.9	9%	335.1	38.2	11%	311.3	44.0	14%
GTE_SCE(1)	-186.5	3.2	-2%	-183.2	8.6	-5%	-156.5	21.5	-14%	-167.8	9.3	-6%	-174.3	6.2	-4%	-179.0	4.4	-2%	-164.8	12.6	-8%	-187.3	8.2	-4%
GTE_SCE(2)	-177.1	10.4	-6%	-193.3	14.0	-7%	-180.9	14.7	-8%	-194.1	16.3	-8%	-243.9	9.1	-4%	-256.5	4.0	-2%	-212.1	17.6	-8%	-244.1	4.8	-2%
GTE_SCE(3)	-174.8	4.5	-3%	-180.9	14.7	-8%	-173.8	18.7	-11%	-199.5	14.9	-7%	-228.2	10.5	-5%	-267.4	17.3	-6%	-293.2	40.5	-14%	-274.9	41.2	-15%

Note: The potential of control chloride probe, rebars, and graphite probes was measured against a SCE, whereas that of the SwRI chloride probes was measured against their closest graphite probe.

It should be noted that the temperature in existing concrete structures would rarely (if ever) reach as high as 104ºF and the use of this relatively high temperature aimed to accelerate the possible oxidation and degradation of the sensing elements once they are embedded in concrete. Similarly, the sensing elements in field concrete would rarely be completely dry. The wetting and drying cycles aimed to capture the effects of moisture fluctuations experienced by the field concrete on the stability of the embedded sensing elements.

During the testing of sensor longevity, instead of periodically measuring the anodic current flowing between the MAS pins (i.e, ΔI_{ij}), we periodically measured the potential difference between the MAS pins ((i.e, ΔE_{ic}, with the central pin as reference). The potential difference between certain MAS pins (e.g., ΔE_{ij}) was not directly measured but was calculated using the following equation:

$$\Delta E_{ij} = \Delta E_{ic} - \Delta E_{jc}$$

All the ΔE values were taken at their absolute values and subsequently the maximum and average ΔE of each MAS probe in a given test solution was monitored on an hourly basis during the weathering cycles (except the drying periods). Note that one of the MAS probes featured 9 identical small pins whereas the other MAS probe featured 3 small pins and 3 large pins due to short-circuiting.

As shown in Figure 2.17a, for the 9-pin MAS, the following three parameters showed strong correlation with the chloride concentration of the simulated pore solutions: (1) *maximum of maximum ΔE*, (2) *maximum of average ΔE*, and (3) *average of average ΔE / standard deviation of maximum ΔE*. The first two parameters peaked in the range of 0.04 to 0.06 M chloride concentration, whereas the 3rd parameter decreased and the rebar potential increased as the chloride concentration increased.

As shown in Figure 2.17b, for the 6-pin MAS, the following three parameters showed strong correlation with the chloride concentration of the simulated pore solutions: (1) *average of maximum ΔE*, (2) *average of average ΔE*, and (3) *average of average ΔE / maximum of maximum ΔE*. The first two parameters peaked in the range of 0.04 to 0.06 M chloride concentration, whereas the 3rd parameter decreased and the rebar potential increased as the chloride concentration increased.

The ratio (standard deviation of maximum ΔE to average of average ΔE) may not have a specific physical meaning, but may serve as a good indicator of localized corrosion. The more active localized corrosion occurs, the higher the variability in the potential differences (ΔE) values measured from the MAS pins, and the higher the ratio (standard deviation of maximum ΔE to average of average ΔE).

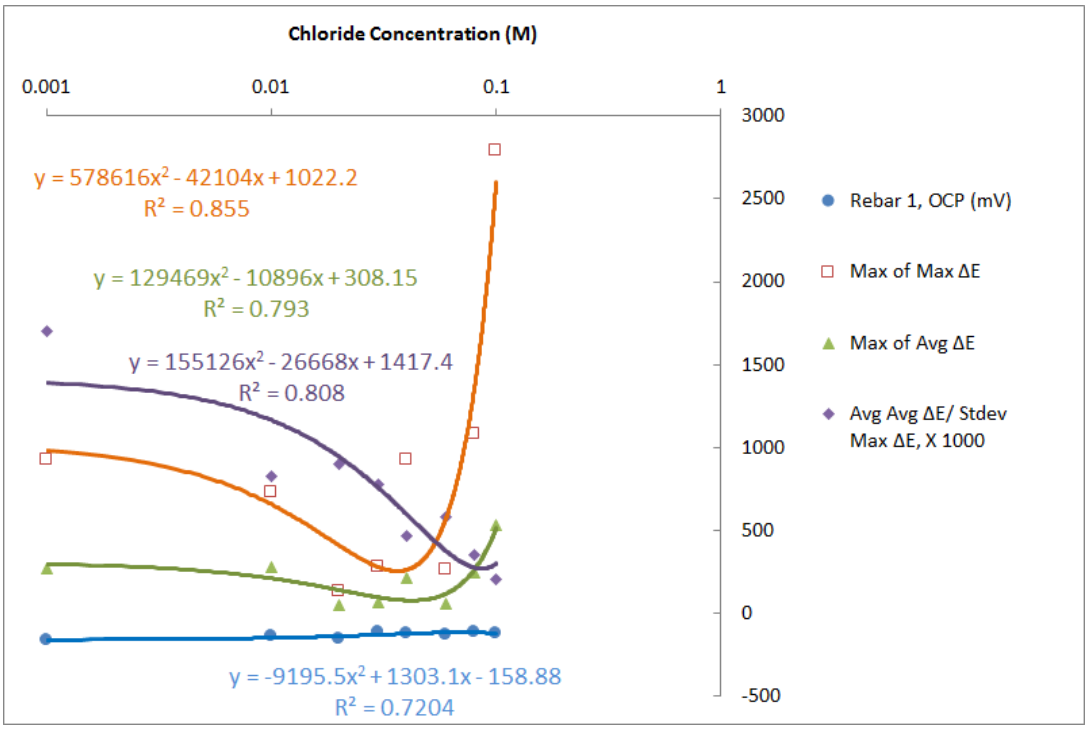

(a)

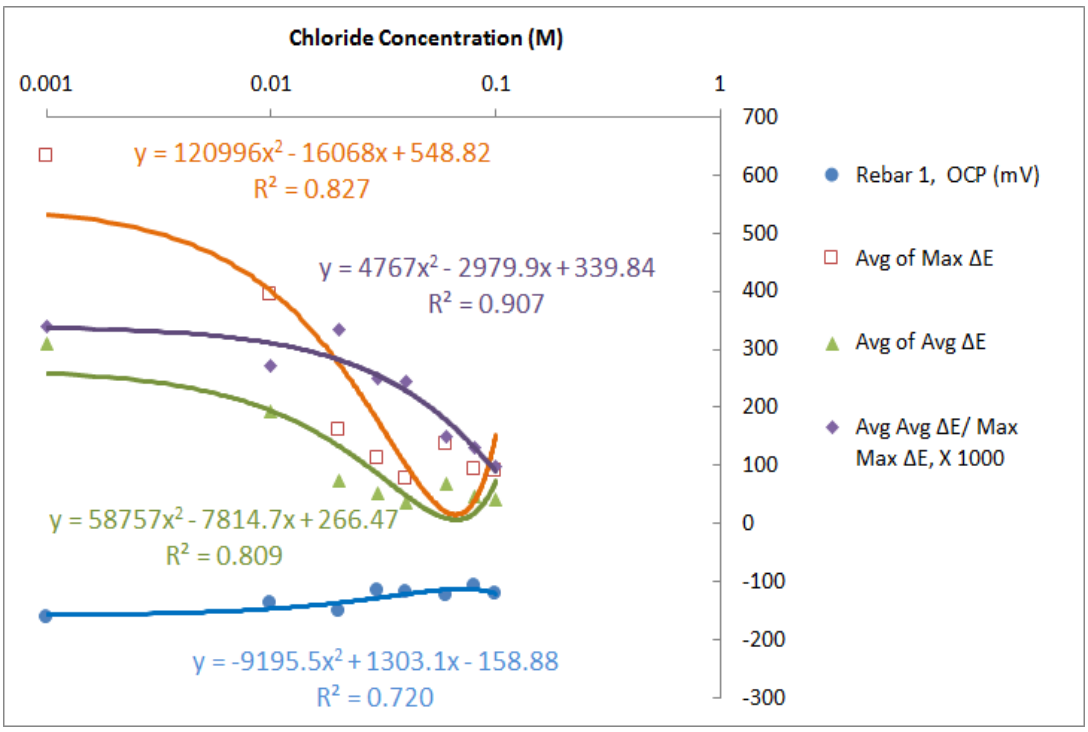

(b)

Figure 2.17: MAS and rebar data as a function of chloride concentration of simulated pore solutions over the eight weathering cycles: (a) MAS with 9 identical pins; (b) MAS with 6 different pins.

As shown in Figure 2.18, for the 9-pin MAS, the following parameter, *standard deviation of maximum ΔE/ average of average ΔE* exhibited a very strong correlation with the chloride concentration of the simulated pore solutions, with R-square of 0.91. This indicated its great potential to be used as a chloride sensor. Yet, neither this nor other parameters from the 9-pin MAS probe exhibited a sufficiently strong correlation with the average corrosion rate of the carbon steel rebars.

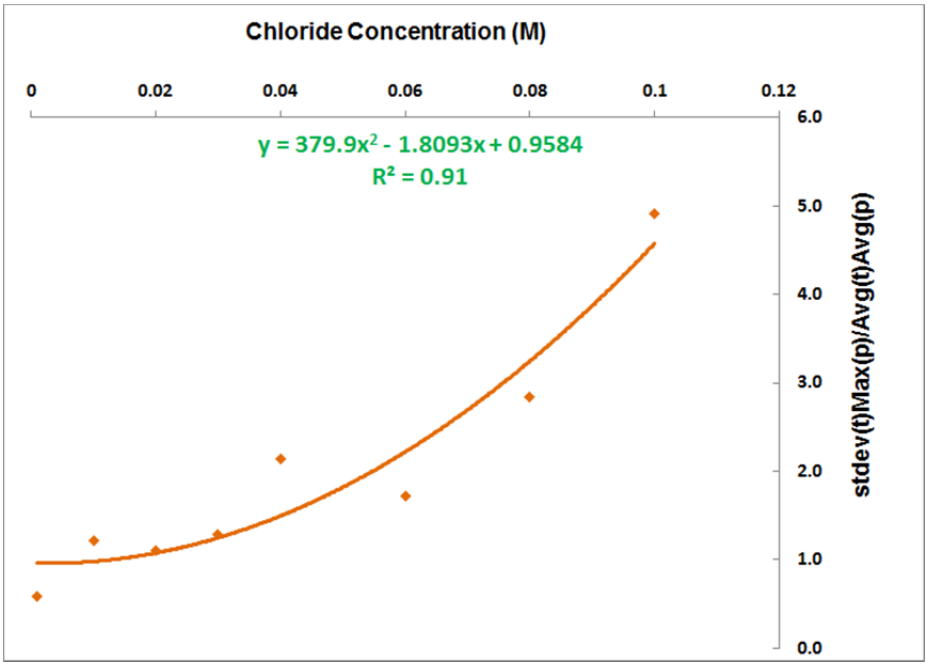

Figure 2.18: Parameters from the 9-pin MAS as a function of chloride concentration of simulated pore solutions over the eight weathering cycles.

As shown in Figure 2.19a, for the 6-pin MAS, the following parameter, *maximum of maximum ΔE/ average of average ΔE* exhibited a very strong correlation with the chloride concentration of the simulated pore solutions, with R-square of 0.97. This indicated its great potential to be used as a chloride sensor. As shown in Figure 22b, for the 6-pin MAS, the following parameter, *standard deviation of maximum ΔE/ average of average ΔE* exhibited a very strong correlation with the average corrosion rate of carbon steel rebars, with R-square of 0.92. This demonstrates the great potential of using the 6-pin MAS as a reliable tool to predict the rebar corrosion rate even in the case of active corrosion and high chloride concentration, which warrant additional research.

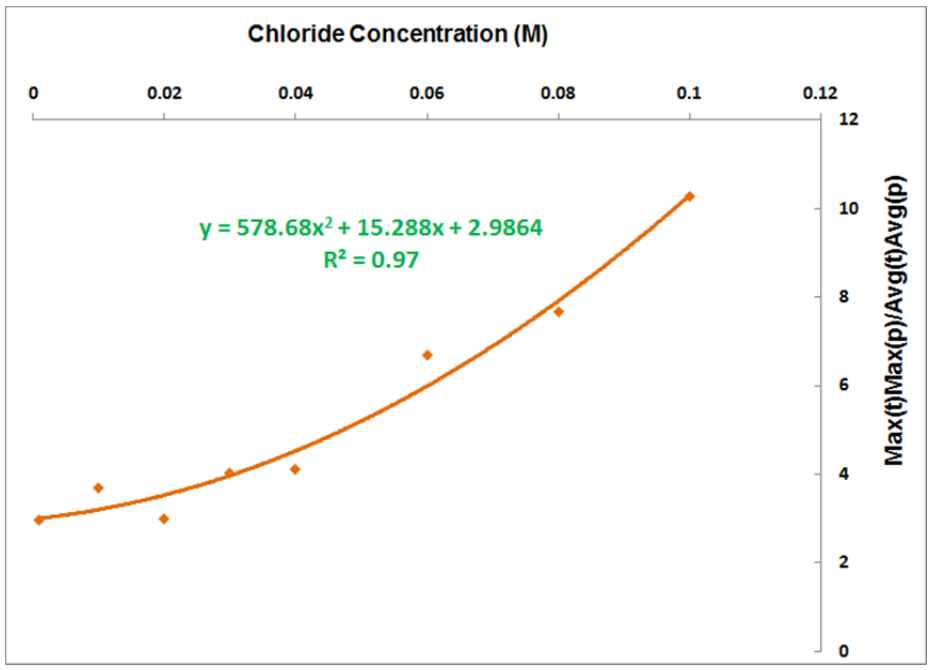

(a)

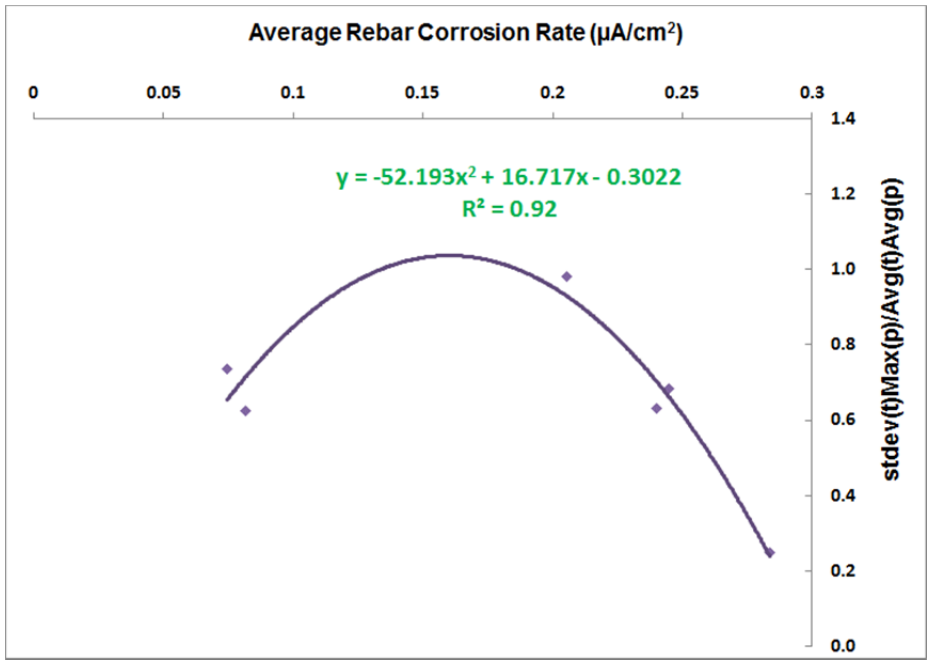

(b)

Figure 2.19: Parameters from the 6-pin MAS as a function of (a) chloride concentration and (b) average rebar corrosion rate in simulated pore solutions over the eight weathering cycles.

As shown in Figure 2.20, only three out of the eighteen WTI custom-made chloride probes (WTI Cl1b, WTI Cl2a, and WTI Cl3) can be considered reliable chloride probes after the eight cycles

of weathering. This is based on the fact that their average potential reading maintained a high 2nd-order polynomial correlation (0.88 or above) with the chloride concentration of simulated pore solution, over the eight weathering cycles. In contrast, two of the three SwRI Ag/AgCl probes (SwRI Cl2 and SwRI Cl1) may be considered reliable chloride probes after the eight cycles of weathering, whereas the SwRI Cl3 probe exhibited a relatively weaker correlation (R-square of 0.795). Note that as the chloride concentration increased, the Cl probe potential generally decreased (except for SwRI Cl3). This was consistent with the theory of electrochemical equilibrium (Nernst Equation).

As discussed earlier (as shown in Table 2.3), the 2nd SwRI chloride probe failed to remain reliable after cycle 6 and showed high COV values during cycles 7 and 8. In other words, only one of the three SwRI Ag/AgCl probes can be considered reliable chloride probes. This highlights the need for further improving the approach to fabricate the Ag/AgCl probes to serve as chloride probes in concrete. Meanwhile, the three WTI custom-made chloride probes (with the appropriate treatment by proprietary coating) showed great promise in this regard.

Finally, as shown in Figure 2.20, the control Cl^- probe (Ag/AgCl via electrodeposition only) failed to exhibit a good correlation between its average potential reading and the chloride concentration of simulated pore solution, over the eight weathering cycles. The R-square in this case was only 0.562, indirectly confirming the superior longevity of custom-made SwRI and WTI chloride probes.

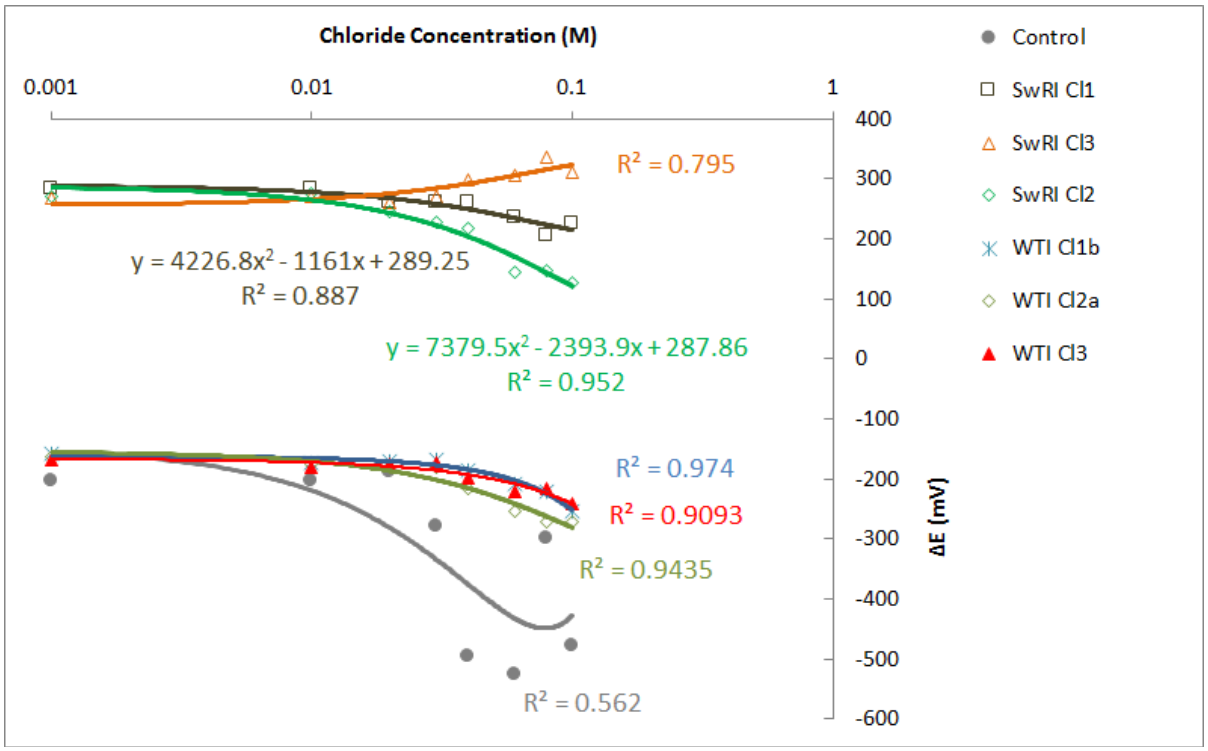

Figure 2.20: WTI and SwRI chloride probes as a function of chloride concentration of simulated pore solutions over the eight weathering cycles

Note that the potential of the control chloride probe and WTI chloride probes was measured against a SCE, whereas that of the SwRI chloride probes was measured against their closest graphite probe. As shown in Table 2. 4, this may have partially contributed to the high variability observed in the measurements by the SwRI chloride probes. Table 4 reveals that over the eight weathering cycles, only one of the SwRI graphite probes (GTE_SCE(1)) remained relatively stable, with its potential showing a standard deviation of 11 mV and a COV of -6%. Interestingly, a few of the WTI custom-made Ag/AgCl probes (WTI Cl1a and WTI Cl1c) showed good possibility to serve as reliable reference electrodes in concrete.

Table 2.4:. Potentiometric responses of the SwRI reference probes and WTI reference probes during the weathering cycles

Cycle	Solution (Cl^-, M)	WTI Cl1a	WTI Cl2b	WTI Cl1c	WTI Cl3	GTE_SCE(1)	GTE_SCE(2)	GTE_SCE(3)
1	0.001	-159.2	-167.2	-266.4	-330.2	-186.5	-177.1	-174.8
2	0.01	-170.0	-179.3	-266.1	-374.3	-183.2	-193.3	-180.9
3	0.02	-156.7	-174.3	-281.9	-358.8	-156.5	-180.9	-173.8
4	0.03	-155.5	-172.0	-269.3	-341.5	-167.8	-194.1	-199.5
5	0.04	-170.0	-197.3	-287.2	-370.9	-174.3	-243.9	-228.2
6	0.06	-171.1	-220.2	-304.7	-367.0	-179.0	-256.5	-267.4
7	0.08	-157.3	-216.9	-276.9	-348.2	-164.8	-212.1	-293.2
8	0.1	-178.3	-241.9	-303.5	-406.4	-187.3	-244.1	-274.9
	COV	-5%	-14%	-6%	-6%	-6%	-15%	-22%
	Average	-165	-196	-282	-362	-175	-213	-224
	Standard Dev.	9	27	16	23	11	31	49

Table 2.5 shows the average, standard deviation, and coefficient of variance (CoV) of electrochemical potential readings of various sensing probes within 60 s of immersion into a simulated pore solution with 0.03M NaCl, with readings taken every 10 s. This sheds light on the response time of the sensing probes. The vast majority of WTI custom-made Ag/AgCl probes (except WTI Cl1b) exhibited rapid response time as their potential quickly stabilized in the test solution. In comparison, the SwRI sensing probes featured a slightly higher variability in their 60-s potential readings, indicating a slightly longer response time. Nonetheless, we can conclude that the vast majority of the sensing probes featured a response time of less than 60 seconds.

Table 2.5: Average, standard deviation, and coefficient of variance of electrochemical potential readings of various sensing probes, over 60 s of immersion into a simulated pore solution with 0.03 M NaCl. Note that most types of WTI sensors exhibited poor reliability after the eight weathering cycles, i.e., average potential reading poorly correlated with the chloride concentration of simulated pore solution and thus highlighted in orange color here regardless of their response time.

Name of the WTI Cl sensor	Average	Stdev	COV	Name of the SwRI sensor	Average	Stdev	COV
Amberlite IRA - 400 Chloride	-826.8	0.4	-0.05%	Surafce sensor 1 -1	-61.5	0.9	-1.5%
Polyethylene Oxide	-266.5	0.2	-0.09%	Surafce sensor 1 -2	-59.7	0.5	-0.9%
WTI Cl1a	-123.7	0.3	-0.22%	Surafce sensor 1 -3	-57.7	0.7	-1.3%
Polytetrafluroethylene	-821.8	0.4	-0.05%	Surafce sensor 1 -4	-55.7	0.6	-1.0%
Poly Vinyl alcohol				Surafce sensor 1 -5	-54.0	0.7	-1.2%
Dextrose (Glucose) Anhyrdous				Surafce sensor 1 -6	-52.1	0.7	-1.3%
WTI Cl1b	-19.3	16.2	-83.88%	Surafce sensor 1 -7	-50.4	0.7	-1.3%
Chitosan	-97.6	0.9	-0.90%	Surafce sensor 1 -8	-48.8	0.7	-1.4%
WTI Cl2a	-95.0	0.7	-0.72%				
Chitosan	-92.0	0.7	-0.77%	Surafce sensor 2 -1	-47.2	0.7	-1.6%
Polyethylene Glycol	-89.3	0.7	-0.78%	Surafce sensor 2 -2	-45.6	0.6	-1.3%
Chitosan	-86.8	0.6	-0.70%	Surafce sensor 2 -3	-43.9	0.7	-1.5%
poly Vinyl Alcohol				Surafce sensor 2 -4	-42.4	0.9	-2.1%
Poly Acrylic acid				Surafce sensor 2 -5	-40.9	0.8	-2.1%
Poly Vinyl Alcohol	-78.9	0.8	-1.03%	SWRI - 1	-39.5	0.9	-2.3%
WTI Cl2b	-76.8	1.0	-1.27%	SWRI - 2	-38.0	0.8	-2.0%
WTI Cl1c	-74.5	0.6	-0.76%	SWRI - 3	-36.7	0.8	-2.2%
WTI Cl3	-72.0	0.6	-0.82%	Control Cl sensor	-63.7	0.5	-0.8%

2.6 METHODOLOGY FOR SENSOR DATA QC AND INTERPRETATION

2.6.1 Algorithm for the Prediction of Remaining Service Life

Reinforcement corrosion induced by chloride contamination is a leading cause of structural damage and premature degradation in RC structures. It is critical to monitor the health status of structures to ensure safety of traffic and transportation infrastructures. The appearance of the first corrosion crack is usually used to define the end of functional service life, under which rehabilitation of associated structures is required (Tuuti 1980, Weyers 1998). Hence, a key element in the evaluation of service life is to predict corrosion cracking (Maaddawy and Soudki 2007).

Tuutti (Tuutti 1980) identified two phases in deterioration caused by corrosion: the initiation phase and the propagation phase. The initiation phase is the time required for sufficient CO_2 and Cl^- ions to reach the steel-concrete interface and activate corrosion. The propagation phase is the time between corrosion initiation and corrosion cracking, in which the accelerated corrosion of

the RC structure ultimately leads to cracking. Weyers (Weyers 1998) further divided the propagation phase into two different periods, the free expansion period and the stress build-up period. Under the propagation phase, a more reactive maintenance strategy would be necessary. Therefore, the prediction of time-to-corrosion-initiation due to ingress of Cl^- ions is crucial.

According to the Fick's second law, chloride ion migration into water-saturated concrete is an ionic diffusion process. Fick's second law represents non-steady state diffusion and is shown by the following partial differential equation:

$$\frac{\partial C}{\partial t} = \frac{\partial}{\partial x}\left(D\frac{\partial C}{\partial x} \right) \tag{2.4}$$

where C = chloride ion concentration
D = diffusion coefficient
t = time
x = depth

Depending on the boundary conditions, the above equation has many solutions. The most common solutions use the boundary conditions of $C(x=0) = C_S$ (constant chloride surface concentration) and C_0 (original chloride concentration in concrete as a constant). Usually C_0 is set as 0. Then Fick's second law becomes:

$$C(x,t) = C_0 + (C_S - C_0)\left[1 - \text{erf}\left(\frac{x}{2\sqrt{Dt}} \right) \right] \tag{2.5}$$

where C(x,t) = chloride concentration at depth x after time t
D = diffusion coefficient
erf = error function

Assuming one-directional diffusion of chloride, the diffusion coefficient can be obtained by using the chloride probes placed at three different depths (Cl_1, X_1,), (Cl_2, X_2), (Cl_3, X_3) as well as the surface chloride concentration (C_s, 0). To calculate the time to corrosion initiation, a critical value of chloride concentration at the rebar depth is used, that is, $Cl_{th}/[OH^-]$ = constant. A constant value of 1.4 is assumed in this study, based on existing literature. Then, Equation 5 becomes:

$$C_{th} = C_0 + (C_s - C_0)\left[1 - erf\left(\frac{X_r}{2\sqrt{DT_{th}}} \right) \right] \tag{2.6}$$

where X_r = rebar depth

Based on Equation 6, the time of corrosion initiation T_{th} can be obtained. The remaining service life of the RC structure is then calculated by:

$$T = (T_{th} - t) + T_{add} \quad (2.7)$$

where $T_{th} - t$ = the time period to corrosion initiation
T_{add} = a constant value (e.g., 3 years in this case, assumed for the time needed for corrosion propagation to concrete cracking).

2.6.2 Qualify control of Sensor Data

Observational data are subject to systematic and random errors. The quality control (QC) of sensor data is an essential first step before using the data for predicting the remaining service life of the RC structure. In this study, corrosion rate, chloride, pH, and temperature sensors were deployed to provide measurements for prediction. QC schemes were developed to make sure that data used for the calculations had acceptable accuracy. Three types of sensor status were used based on data quality control: normal, questionable, and malfunctioning.

For the corrosion rate sensor, the following rules were developed:

- If the corrosion rate value (CR_n) is negative, then the status is malfunctioning.
- If the corrosion rate jumped from a value smaller than 0.1 $\mu A/cm^2$ (measured at the last time interval) to one greater than 1.0 $\mu A/cm^2$ (measured at current time interval), then flag the sensor status as questionable.
- Predict the corrosion rate value (CR_n') based on the values developed in the previous time intervals (1,2,…, *n*-1), by using polynomial regression. If the measured corrosion rate value (CR_n) deviated more than 50% from the predicted value (CR_n'), then flag the sensor status as questionable.
- Otherwise, the status is normal. Under normal status, the status of corrosion is "passive" if the corrosion rate value is less than 0.1 $\mu A/cm^2$; "transitional" if the value falls between 0.1 and 1.0 $\mu A/cm^2$; and "active corrosion" if greater than 1.0 $\mu A/cm^2$.

For the temperature sensor, if the reading is out of the range of (-35°F, 105°F), then the sensor status is questionable. If no readings available, the sensor is malfunctioning.

For the pH sensor, if the reading is out of the range of (8, 13.8), then the sensor status is questionable. If no readings available, the sensor is malfunctioning.

For chloride probes, a two-phase quality control scheme was developed.

Phase 1:

1. At time interval *n* (or time t_n), assume all three sensors are working normally.

2. If the chloride concentration for a given sensor is negative (or null value), then the status is malfunctioning.

3. If the chloride concentration for a given sensor is greater than 2.0 M, then the status is questionable (this could indicate a dry condition of the concrete near the sensor).

4. If at least two sensors are marked as normal, apply the data to Equation 2 to obtain the diffusion coefficient (D_n) at time interval *n*. Predict the diffusion coefficient value (D_n') based on the diffusion coefficient values developed in the previous time intervals (1,2,…, *n*-1), by using polynomial regression. If the measured chloride diffusivity (D_n) deviated less than 50% from the predicted value (D_n'), then finish data quality control. Otherwise, continue to Phase 2.

Phase 2:

1. If three chloride and corrosion rate sensors are all normal, use Table 2.6 to update the calculation of the remaining service life, $T_{th(n)}$, at the measurement time interval t_n.

Table 2.6: Remaining service life $T_{th(n)}$ (with three normal chloride sensors, and normal corrosion rate sensor)

	$CR_n < 0.1$	$0.1 < CR_n < 1$	$CR_n > 1$
$T_{th(n)} > t_n$	$T_n = T_{th(n)} - t_n + T_{add}$	$T_n = T_{th(n)} - t_n + T_{add}$	If $T_{n-1} > t$, $T_s = T_{th} - t + T_{add}$ Otherwise, $T_n = T_{add}$ (Chloride probe status is further set as questionable.)
$T_{th(n)} \le t_n$	$T_n = T_{n-1} - (t_n - t_{n-1})$ (Chloride probe status is further set as questionable.)	$T_n = T_{add}$	$T_n = T_{add}$

If corrosion rate sensor is not normal, $T_n = T_{th(n)} - t_n + T_{add}$.

2. If two chloride probes and the corrosion rate sensor are normal, use Table 2.7 to calculate service life.

Table 2.7: Remaining service life $T_{th(n)}$ (with two normal chloride sensors, and normal corrosion rate sensor)

	$CR_n < 0.1$	$0.1 < CR_n < 1$	$CR_n > 1$
$T_{th(n)} > t_n$	$T_n = T_{th(n)} - t_n + T_{add}$	$T_n = T_{th(n)} - t_n + T_{add}$	$T_n = T_{add}$ (Chloride probe status is further set as questionable.)
$T_{th(n)} \le t_n$	$T_n = T_{n-1} - (t_n - t_{n-1})$ (Chloride probe status is questionable.)	$T_n = T_{add}$	$T_n = T_{add}$

If corrosion rate sensor is not normal, $T_n = T_{th(n)} - t_n + T_{add}$.

3. If only one chloride probe and the corrosion rate sensor are normal, use Table 2.8 to calculate service life.

Table 2.8: Remaining service life $T_{th(n)}$ (with only one normal chloride sensor, and normal corrosion rate sensor)

	$CR_n < 0.1$	$0.1 < CR_n < 1$	$CR_n > 1$
$T_{th(n)} > t_n$	$T_n = T_{n-1} - (t_n - t_{n-1})$	$T_n = T_{n-1} - (t_n - t_{n-1})$	$T_n = T_{add}$ (Chloride probe status is further set as questionable.)
$T_{th(n)} \le t_n$	$T_n = T_{n-1} - (t_n - t_{n-1})$ (Chloride probe status is questionable.)	$T_n = T_{add}$	$T_n = T_{add}$

4. If no chloride probe is normal and the corrosion rate sensor is normal, use Table 2.9 to calculate service life.

Table 2.9: Remaining service life $T_{th(n)}$ (with no normal chloride sensors, and normal corrosion rate sensor)

$CR_n < 0.1$	$0.1 < CR_n < 1$	$CR_n > 1$
$T_n = T_{n-1} - (t_n - t_{n-1})$	$T_n = T_{n-1} - (t_n - t_{n-1})$	$T_n = T_{add}$

If the corrosion rate sensor is not normal, then $T_n = T_{n-1} - (t_n - t_{n-1})$

Note that the current QC algorithms assume one-directional diffusion of chloride into concrete and the chloride probe 3 at the depth of the rebar of interest. As such, the algorithms will need to be modified for the case of ODOT concrete girder, which features two-directional diffusion of chloride into concrete and the embedment of chloride probe 2 at the depth of the rebar. The current QC algorithms, however, have laid the groundwork for further improvements of the software.

2.6.3 Software Interface

A software package is developed based on the algorithms and data QC schemes provided above. The main interface is shown in Figure 2.21, which includes (remaining) service life prediction, sensor status, and display of historical data.

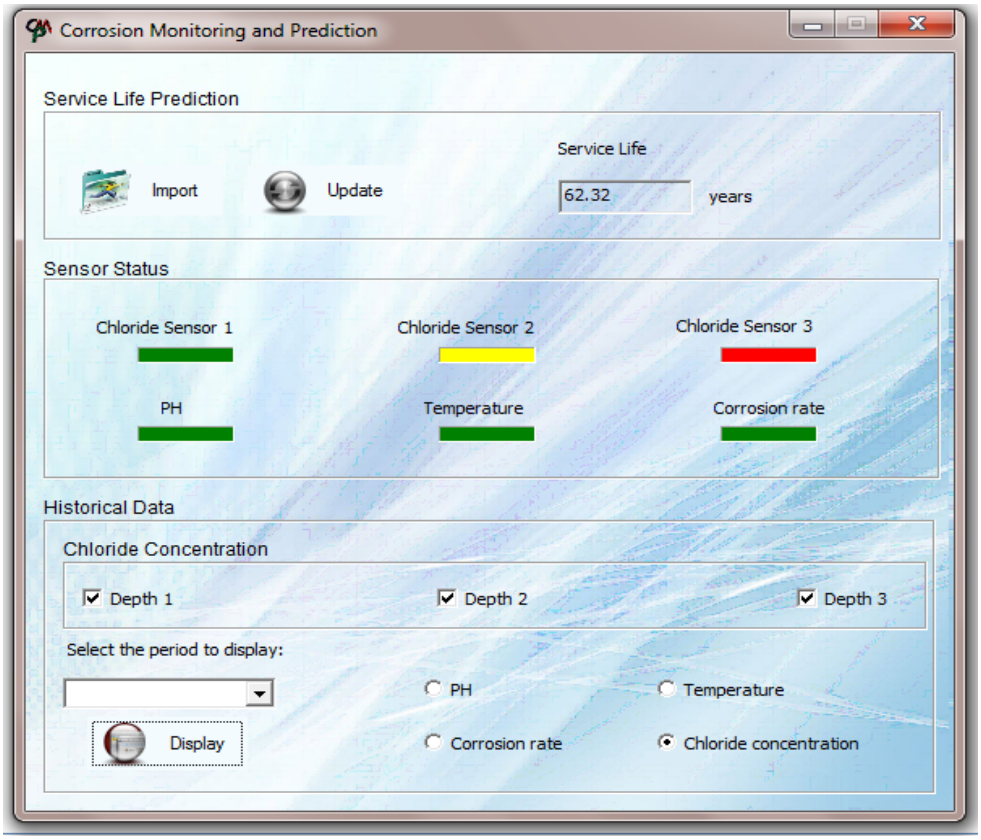

Figure 2.21: Main user interface of the corrosion sensing system

Under Service Life Prediction, the "Import" button (

) allows users to open, select, and import new data set that will be incorporated into the analysis. When the mouse cursor is over the "Import" button, the software shows the hint: " 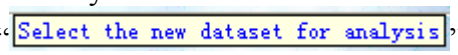

".

The "Update" button (

) is to calculate and update the service life of the associated infrastructure and the result is shown the under the text "Service Life" (

).When the mouse cursor is within the "Update" button area, the software shows the hint: " 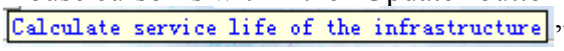

".

Under the sensor status section, the interface displays the status of the three chloride probes, pH sensor, temperature sensor, and corrosion rate sensor. Sensor status include "normal" (indicated by green bar, such as 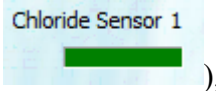

), "questionable" (indicated by yellow bar, such as 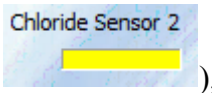

), and "malfunctioning" (indicated by red bar, such as 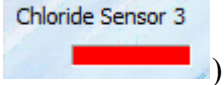

).

The software also provides access to historical data for all of the sensors. By selecting the sensor (Chloride Concentration, pH, temperature, etc.) and time period (30 days—30D, 90D, 180D, 1Y, 3Y, 5Y, ALL), clicking on the “Display” (

) button, a pop-up window shows the desired historical data.

3.0 INTERPRETATION, APPRAISAL, AND APPLICATIONS

3.1 GUIDELINES FOR SENSOR FIELD IMPLEMENTATION

This section describes in detail the components included in the delivered system and the steps necessary to successfully install the system in field location. It takes operators from the steps of identifying the parts that are sent to the field and how to install everything from the wire connection between parts to successfully acquire data from the system.

3.1.1 Parts for the Corrosion Sensing System

The summary of the components in the corrosion monitoring system is listed in Table 3.1.

Table 3.1. Components included in the delivered corrosion monitoring system

No.	Item & Description
1	1 x Sensor Set Includes: 1) three chloride probes and three graphite reference probes; 2) two 9-pin MAS probes and 3) one thermometer probe. The picture of the sensor is shown in Figure 3.1
2	1 x Aginova Sensor Platform (with supportive plate) Includes: 1) One Aginova MAS board (sensor ID: 8141) and 2) Two Aginova Sentinel Chloride board (Sensor ID: 9216 and 9226). The picture of the platform is shown in Figure 3.2
3	1 x NETGEAR Wireless-G Router (WGR6 14 v9) The picture of the router is shown in Figure 3.3
4	1 x Laptop (Dell Latitude D531 Laptop) and 1 x Aginova Software (Gold Version) The picture of the laptop with Aginova software is shown in Figure 3.4
5	1 x APC Back – UPS The picture of the UPS is shown in Figure 3.5
6	1 x Wire Cable connecting Router to Laptop (see Figure 3.6)
7	1 x Wire Cable connecting Router to UPS (see Figure 3.6)
8	4 x Battery for MAS board The picture of the battery is shown in Figure 3.6
9	8 x Battery for Chloride Board The picture of the battery is shown in Figure 3.6

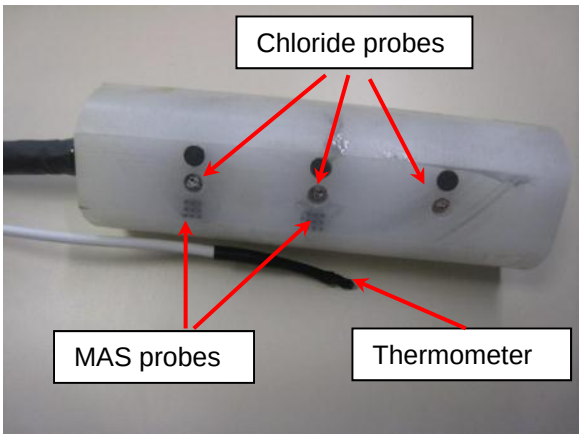

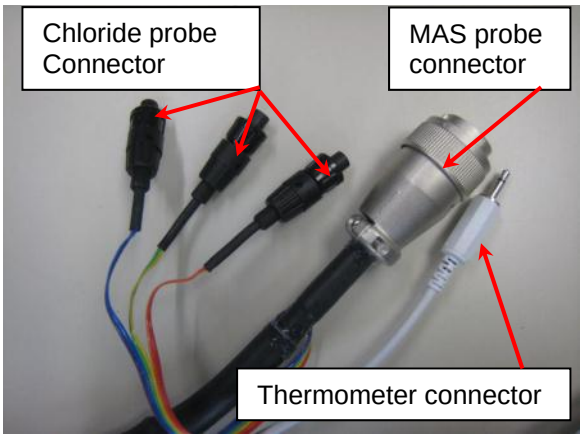

(a) (b)

Figure 3.1:Corrosion monitoring sensor. (a) sensor body and (b) connectors

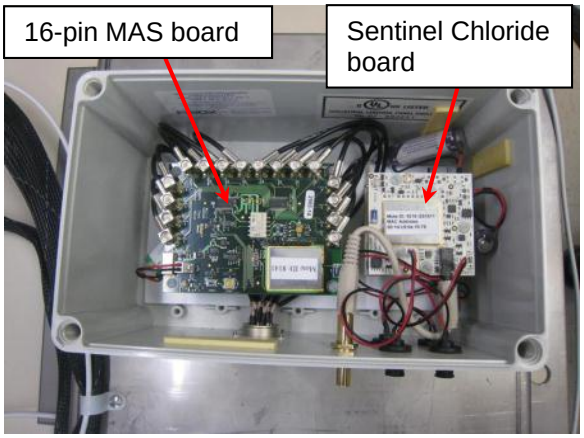

(a) (b)

Figure 3.2:Aginova Sensor Platform (with supportive plate) (a) top view and (b) front view

Figure 3.3: NETGEAR Wireless-G Router (WGR6 14 v9)

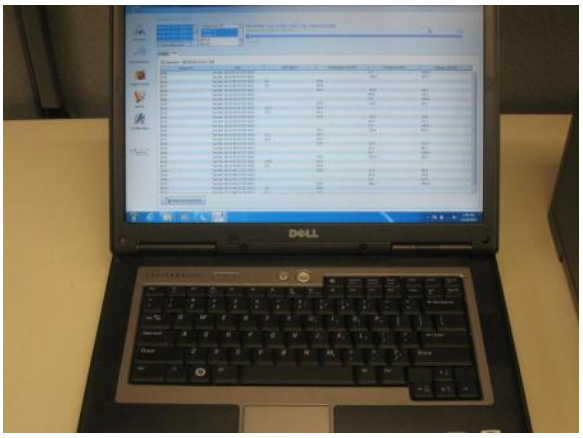

Figure 3.4:Laptop (Dell Latitude D531 Laptop) with Aginova Desktop Software (Gold Version) embedded

Figure 3.5:Power supplier (APC Back – UPS) for the Router

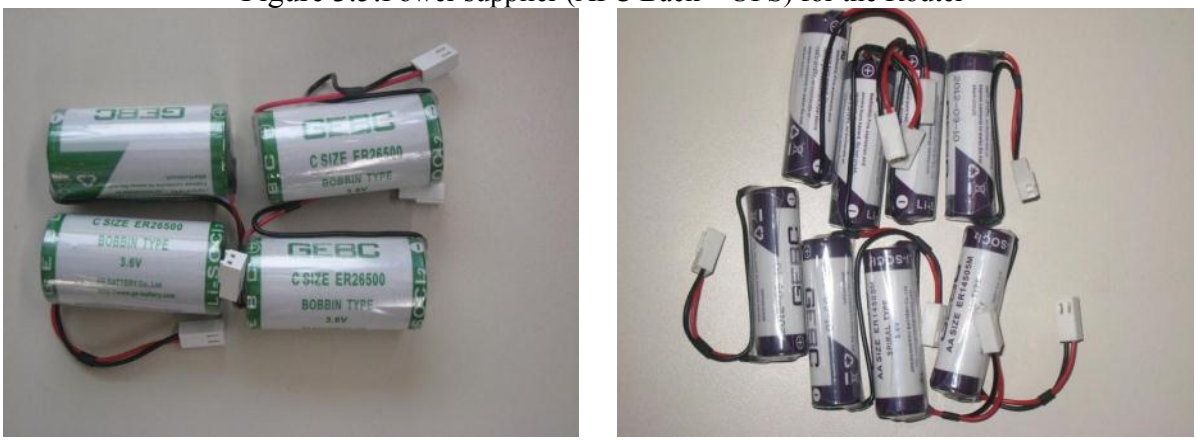

(a) (b)

Figure 3.6: Backup batteries (a) for MAS board and (b) for chloride board

3.1.2 Step-by-step Field Implementation Procedure

The detailed procedure for field implementation is described as follows.

1. Identify the components in the system and check the sensor platform

   Once the system is delivered, the DOT engineer should unwrap the box and identify the components in the delivery. Although well packed before shipping the platform, the components within the platform box may move and dislocate from the appropriate location due to the vibration in the shipping process. After delivery, operator should open the platform box to check if the components and wire connection are well fixed in the appropriate location.

   After delivery, the integrity of sensor set should be carefully checked. If there is integrity issue regarding the sensor body or the connectors, please contact engineer at SwRI. If sensor probe surface is contaminated, please slightly polish with fine sand paper and then clean with DI water.

2. Install the batteries into the board

   To avoid board batteries moving and breaking the board during the shipping process, the batteries were removed before shipping and will be shipped separately. Therefore, the batteries need to be reinstalled and the system reset before monitoring. The re-set process is described below in detail and a document with a video demonstration of the installation process is included with the deliverables. Note that one battery for each individual board will be reinstalled for each of the three boards.

   The large “C” type batteries in a separate plastic bag will be used for the 16-pin MAS board and the “AA” style batteries in another plastic bag will be used for the chloride boards. All batteries are wired with an appropriate connector. In the installation, first, the four screws on the cover of the platform should be removed with screw driver. Prior to installing the battery, please double check that the switch on each board is in the “off” position. Next, use the screwdriver to remove the four screws that holds down the upper chloride board. Then remove the upper chloride board from the box carefully. Subsequently, remove the four standoffs on the lower chloride board with a screwdriver and take out the lower chloride board from the box.

   A connector for the battery can be found at the bottom side of the lower chloride board. Attach one “AA” type battery to the connector. Put the board back in and fix the battery with a tape. Screw the four standoffs back to the lower board. Then attach another “AA” type battery to the upper board through the connector at the back side of the board and then place the board back in. Mount the four screws on with the screwdriver. Double check if the two chloride boards are fixed in the appropriate location.

   A connector on the front side of the MAS board can be found. Connect the “C” type battery to the MAS board through the connector. Turn all switches of three boards from “off” to “on” and the green LED lights on the three boards should be “on” momentarily.

A screwdriver may be needed to help turn the switches on the chloride boards to “on”. If the LED light on a specific board does not indicate “on”, please check the battery connection and re-connect it if necessary. In the end, put the cover back on and tighten the screws.

3. Wire connect components within the system

This work includes two parts. One is connecting the sensor set with the platform and the other is wire connecting the router, the laptop and the power supply, UPS. An included video demonstrates the connection process.

First, check the compatibility of the sensor connectors with the connectors embedded in the platform. Note that only three chloride probe connectors are weather proof, but the connectors for the MAS and thermometer probes are not weather proof. The MAS and thermometer probes should be sealed with electrical grade silicone (does not contain acetic acid) after connecting.

Plug the 16-pin round MAS sensor connector (military connector) into the platform box. Push the MAS connector fully in and tighten the connector. The connection between the chloride probe connectors and connectors on the platform box can be identified with the color code of the connector wire and written on the platform box. Put the notch of the sensor wire connector in a line with the notch of the connector in the box. Then push it in, spin until it clicks. The pin connector for the temperature sensor is connected by pushing straight in the connector on the box. The RED wire transfers data from the top chloride probe, which is close to the connection wire. The GREEN and BLUE wires transfer data from the middle and bottom chloride probes, respectively.

Figure 3.7 shows the wire connection for the router, laptop and UPS. Note that the UPS should be fully charged (charge at leastfour hours and preferably overnight) before each field usage. Our test indicates that the UPS can continuously supply power to the router for more than 5 hours, which is more than enough for the router to communicate with the platform and download two-years of data stored on the board. During operation, the UPS gives an audible noise every couple minutes, which indicates it is not connected to an AC power source. This is normal and no action should be taken. Also note that during the field data acquisition process, the components, including laptop, router and UPS, should be placed less than 100 feet from the platform.

The network cable wire connects the laptop and the No.1 connector of the router. The power wire will be plugged to the router and the battery side of the UPS. Turn on the laptop. No user name and password have been pre-set for this laptop. Double click the icon “Aginova” on the desktop and the software interface shown on the screen. Note that the laptop uses its own battery in field operation. The UPS only provides power to the router. The router will pick up all data collected and store in the platform in a specific time interval.

(a)

(b)

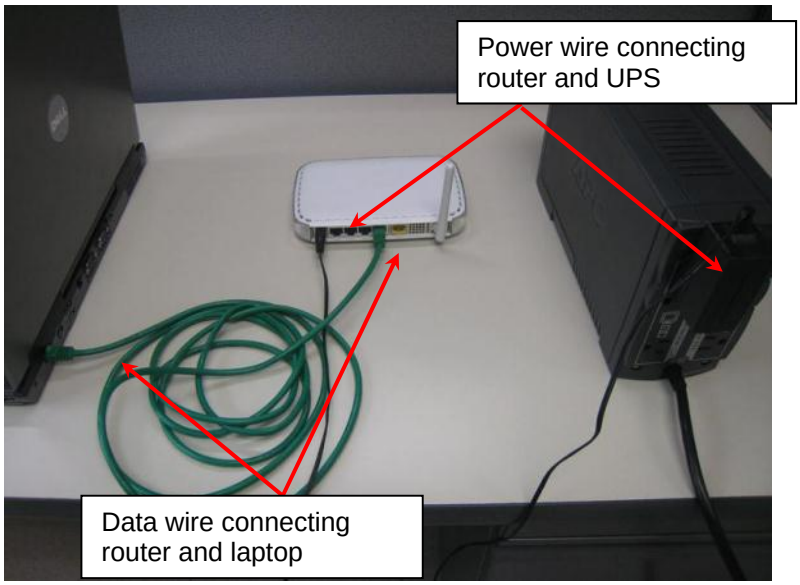

(c)

Figure 3.7: Wire connection for router, laptop and the UPS (a) router (back view), (b) UPS (back view) and (c)

4. Install sensor body and platform

   In the bridge structure, select a location that represents the most severe chloride attack and rebar corrosion occurrence to embed the sensor body. A cylindrical hole with 2 ½" diameter and 6″ depth should be drilled at the selected location. The hole should be 45° downward relative to the surface of the structure. The sensor body will be fully embedded in the middle of the hole. The paste provided by Montana State University will be used to fill the space between sensor and the structure tightly. Note that when embedding the sensor body into the structure, the flat surface with probes must face toward the concrete surface. Also note that no rebar should touch the sensor directly.

   The platform will be placed near the embedded sensor body. To avoid the stress on the connection wires, the distance between the platform and the sensor should be less than 5 feet. Further, the platform should be placed in a shielded space. The platform will be fixed on a flat surface of the structure through mounting the supportive plate with four 5/8" bolts. After mounting the plate, open the platform cover and turn the power switch button on. Then tightly screw down the cover to seal the platform.

5. Test the workability of the system

   To test the workability of the whole system, the acquisition frequency for data from all probes is pre-set at three minutes in the software when the system is delivered. Therefore, after the batteries are installed and the power switch for the boards turned on, the platform starts to pick up data from the three boards several minutes later. In each three-minute interval, there are a total of 16 "click" noises from the platform, which indicates

that the MAS board is picking up data from MAS probe. Similarly, the chloride boards pick up data from chloride probes and the thermometer probe every three minutes but with no noise heard.

Turn on the laptop and double click the "Aginova" program. After approximately 10 minutes, click the "List of Sensors" icon on the left. All available sensors, including the MAS sensor, the three chloride probes and the one thermometer, will be listed. A sensor that appears in green text is in communication with the software. If a specific sensor appears black, it is not responding to the communication inquiry from the router. If a sensor is not responding, the following check process should be performed in sequence. 1) check that the probe and the platform wires are securely connected; 2) check that the power button on the board is "on"; and 3) check that the UPS and battery of the laptop work. If there is still no response in half an hour, shut down the laptop and unplug the cables. Repeat the process from the beginning. If is still doesn't work, please contact SwRI personnel for help.

It is to be noted that the data of the MAS probe shown in the software are the raw data of each individual electrode. The data columns 0-7 represent raw data from electrodes 0 to 7 and the data columns 8-16 represent raw data from electrodes 8 to16. The two groups of data represent the results of the top and middle of the MAS probe, respectively. The data needs to be downloaded, exported to a spreadsheet, and the calibration equations applied in order to get rebar corrosion rate and mass loss.

If the communication test is successful, adjust the data acquisition frequency for all sensor probes to 6 hours, which will provide enough data for subsequent analysis and a longer battery life. When all available sensors are "green" change the acquisition rate by checking the box next to one or up to all sensors then click the "configure selected sensors" button at the bottom of the screen. A new window will open up with various options to change. Input a new time interval in the "sampling period" in seconds to change acquisition rate. Note that the unit of input time interval is seconds. If the sampling period is 6 hours, the input data should be 21600. When ready to change click the "schedule reconfiguration" button at the bottom to initiate reconfiguration. It will take several minutes for the reconfiguration to be performed on the sensor(s). To verify that the sensor(s) has been reconfigured, go to "List of Sensors" and click the sensor you wish to check. The details regarding the sensor will be highlighted and displayed on the screen. "Sampling" is the sampling rate for that sensor.

Once system passes the testing, the data acquisition components, including laptop, router and UPS will be shut down and disconnected for the next field data collection. It is expected that the DOT engineer visit the site and download the data every 3 months.

6. Download data periodically

For each onsite visit, the DOT engineer will bring the router, USP and laptop to the field to check the workability of the system and download data stored on the boards. As described in step 3), connect the router, USP and laptop; turn on the laptop, and open the software. The "Overview" interface appears first. Click the "Graph and Data" icon on the

left of the screen to switch to the data view. Click the "Data" Tab to see the spreadsheet style view of the data. Select all available sensors from the sensor list box. Select all available data types from the data type list box. Next select the time period you wish to see from the option tab on the top of the interface. The slide bar can be used to further refine the time period of data you wish to view. Allow the data to update and then click the "Export to Excel" Button at the bottom of the software. Input a name to the file a name and click "save". The data file can be sent to SwRI and MSU for analysis and discussion.

3.2 THE SENSOR EMBEDMENT METHOD

Various mortar mixes were designed and tested for their potential use for embedding the corrosion sensing system. Experimental testing focused on the workability and initial setting time of fresh mortar mixes, the 28-day compressive strength of hardened mortar mixes as well as their modulus of elasticity, bond strength on old concrete, chloride diffusion coefficient, and coefficient of thermal expansion. A comprehensive examination of the experimental data led to the selection of two highly flowable, self-consolidating mortar mixes for embedding the corrosion sensing system.

The sensor assembly was installed in a hole drilled at a 45^{o} downward angle near the bottom of a concrete pier. The extracted core was tested to assess the chloride concentration profile of the existing concrete.

The sensor embedment method is illustrated in Figure 3.8. The primary goal was to minimize the potential disturbance of embedment on the local environment to be monitored. A total of three materials were used sequentially for embedding the corrosion sensing. These included: mortar mix 1B, mortar mix 1A and marine epoxy. Both mortar mixes were highly flowable in their fresh state once mixed correctly; their hardened-state compatibility with existing old concrete had been validated in the WTI laboratory.

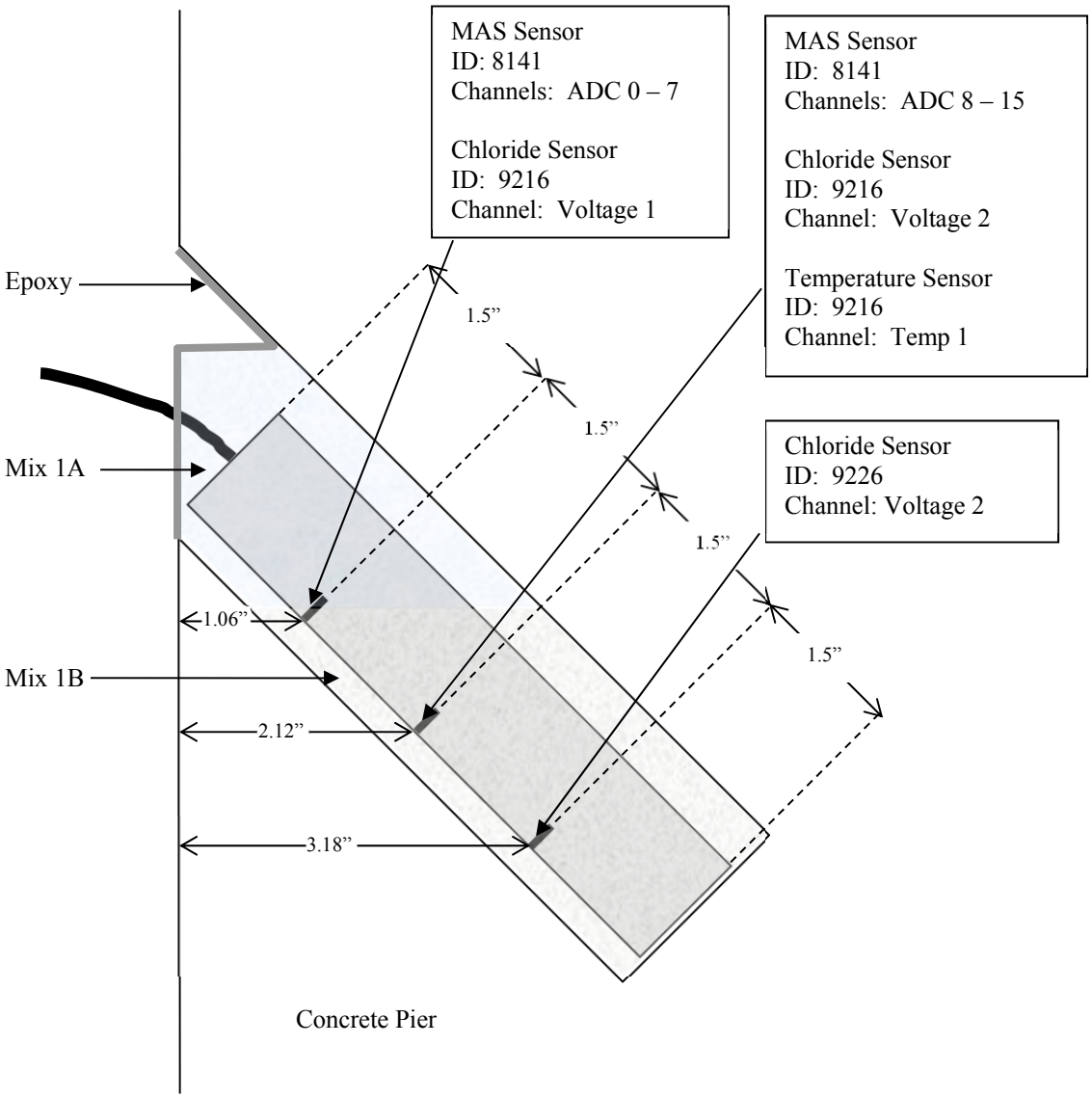

Figure 3.8: Schematic illustration of the sensor embedment method

The sensor assembly was embedded based on the following procedure:

Step 1. Drill four small holes (e.g., 1/8" in diameter and depth) on the white polypropylene cylinder body of the corrosion sensing system. Avoid areas with exposed sensing elements. Drill these four holes at various depths and sides of the cylinder. Do not drill too deep so that the interior of the sensor wires are free from potential damage by the drilling.

Step 2. In each of these drilled small holes push in a plastic cylinder (1/8" in diameter and 5/8" in depth). Note that this leaves separation between the sensing elements and the inside (surface) of the hole" to be 0.5" and the mortars will be able to flow through such "crevices".

Step 3. Clean the drilled hole in the concrete with paper towel and compressed air to ensure that the surfaces are free of debris, free water or other contaminants. Push the corrosion sensing system (now with four small plastic plugs protruding out) all the way into the hole where the concrete girder was cored (the hole is 2.5" in diameter and 5" deep and 45 degrees downward facing the ground). Make sure that the sensor side with all the sensing elements is facing the concrete surface.

Step 4. Now that the corrosion sensing system is fixed inside the hole in the concrete element, sealing of the hole can begin.

Step 5. First, mix the solid and liquid components of Mix 1B together (consisting of water, cement, fine sand, carbon microfiber and nanoclay) and add a certain amount of calcium chloride ($CaCl_2.2H_2O$) into it. The appropriate amount is based on the measured chloride concentration profile of the concrete core taken from the girder. Agitate for 10 minutes to obtain best possible uniform distribution of various components. Note that only about 206 mL of this fresh mortar mix 1B (roughly estimated to be 495 g) is poured into the concrete hole, with the goal of just embedding all the sensing elements yet leaving room in the hole for the other embedding materials. This adds a layer of highly permeable mortar to embed the sensing elements, which allows quick equilibrium of chloride content with the adjacent concrete. The volume of 206 mL (highly permeable mortar) is able to fill in the hole for about 3.2" if the hole is not 45 degrees but rather straight.

Step 6. Leave this 1st mortar mix (1B) to flow flat and set in the field for at least 6 hours before proceeding to the 2nd mortar mix (1A).

Step 7. Second, mix the solid and liquid components of Mix 1A together (consisting of water, cement, fine sand, carbon microfiber, nanoclay, SBR, TEA, and calcium nitrite). Agitate for 10 minutes to best possible uniform distribution of various components. Note that only about 129 mL of this fresh mortar mix 1A (roughly estimated to be 309 g) is poured into the concrete hole (on top of the set 1st mortar mix), with the goal of adding a layer of highly impermeable mortar that would minimize the ingress of external chlorides, moisture and other contaminants into the concrete. The volume of 129 mL (highly impermeable mortar) is able to fill in the hole for about 2" if the hole is not 45 degrees but rather straight.

Step 8. Leave this 2nd mortar mix (1A) to flow flat and set in the field for at least 12 hours before proceeding to the 3rd materials (marine epoxy).

Step 9. Third, pour about 58 mL marine epoxy into the hole (on top of the set 2nd mortar mix). This is to further minimize the ingress of external chlorides and moisture into the concrete.

Even before the epoxy sets (typically after 24 hours), the embedment is complete and the embedded sensing system is ready for tests.

3.3 FIELD IMPLEMENTATION ON AN ODOT BRIDGE PIER

This section summarizes the key findings from the field implementation of the SwRI corrosion sensing system on an ODOT bridge pier near the coast. The sensor system was fabricated by the SwRI and delivered to the ODOT for field deployment, along with a system setup and installation manual (with instructional videos). The system was installed on July 1-3, 2013 on a Yaquina Bay Bridge pier with the sensor angled at 45 degrees and located midway across the width of the pier. The installation details are illustrated in Figure 3.8. For this specific bridge pier, the ingress of external chloride into the concrete can be treated as one-dimensional (1-D). The ODOT research coordinator took periodic field trips to the site to download the sensor data. Communication with the 9216 and 9226 boards was lost sometime after the August 2013 download, so only the August 2013 data set has data for all sensors. This highlights the need to improve the electronics package for field applications. The last set of sensor data downloaded was from December 2013 since the communication to all three boards was lost thereafter.

The limited amount of field monitoring data were explored. Based on the Nernst Equation, the chloride concentration and the chloride probes' potential reading was assumed to follow the relationships below.

$$\text{LN } [\text{Cl-}]_t \text{ by sensor 1} = -\text{LN}(t) \times c_1 \times 297.04/(T_t \text{ in K}) * E_{1(t)} + b_1$$
$$\text{LN } [\text{Cl-}]_t \text{ by sensor 2} = -\text{LN}(t) \times c_2 \times 297.04/(T_t \text{ in K}) * E_{2(t)} + b_2$$
$$\text{LN } [\text{Cl-}]_t \text{ by sensor 3} = -\text{LN}(t) \times c_3 \times 297.04/(T_t \text{ in K}) * E_{3(t)} + b_3$$

To obtain the values of b_1, b_2, and b_3, each chloride probe's initial potential reading (an average of three readings in the first day, i.e., at the assumed t of 0 s) was employed. At time zero (t of 0 s), the initial chloride concentration can be estimated as follows. The existing chloride content of the specific ODOT bridge pier was assessed to be about 0.01% by mass of the existing concrete, based on the chemical analysis of the core. As such, $CaCl_2.2H_2O$ was added at 0.01% by mass of the embedding cement mortar. Specifically, about 0.69 g $CaCl_2.2H_2O$ (i.e., 0.0094 mol Cl^-) was added into 1000 mL mixing water, which produced about 6920 g fresh mortar. Assuming 50% of the chloride anions and 90% of the free water were bound, there is about a 0.046 M initial concentration of free chlorides. With this estimated initial free chloride concentration, the values of b_1, b_2, and b_3 can be estimated to be -0.5826, 1.1364, and 4.2786, respectively.

For the field deployed chloride probes inside the concrete, oxidation of the probes by the high-alkalinity inside the concrete was considered in the equations that convert the probe potential readings to free chloride concentration results. Specifically, the values of c_1, c_2, and c_3 were estimated by trial and error so that the majority of the $[Cl^-]$ sensor readings would fall in the range of 0.046 M to 1 M during the first 35 days. With this trial-and-error method, the values of c_1, c_2, and c_3 were estimated to be -0.00614, -0.00184, and -0.00307, respectively.

Figure 3.9 illustrates the temporal evolution of estimated free chloride concentration at various depths of the concrete by the three chloride probes, respectively. Two main patterns can be derived from these chloride probe readings. First, there are great fluctuations of free chloride concentration readings, which may be attributable to the wet/dry cycling inside the concrete. Second, despite the periodical fluctuations, there seems to be an overall trend of chloride concentration increase with time at the depth of probe 1 and probe 2. In contrast, probe 3 did not

illustrate such increase of free chloride concentration over time. These field data reveal the difficulty to implement quality assurance of the chloride sensor readings inside the field concrete and the great difficulty to use such noisy data for prediction of the remaining service life of the reinforced concrete structure. A moisture sensor at the same location of each chloride probe might help clarify the effect of moisture level on the free chloride concentration readings and mitigate these difficulties.

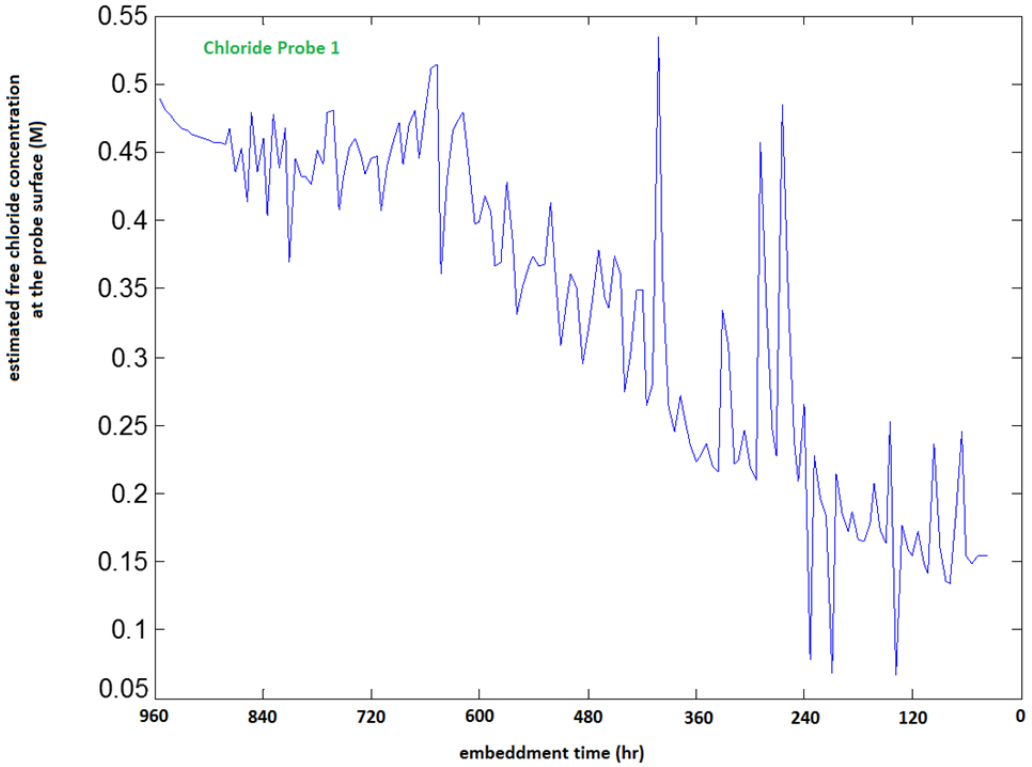

a) Chloride Probe 1

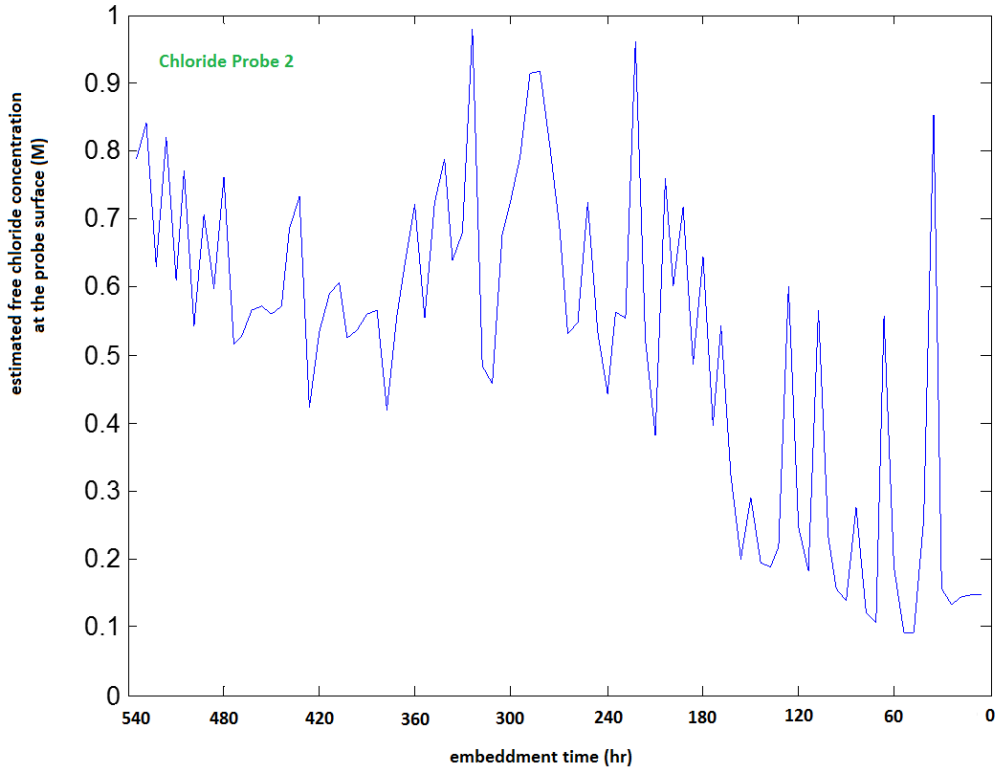

b) Chloride Probe 2

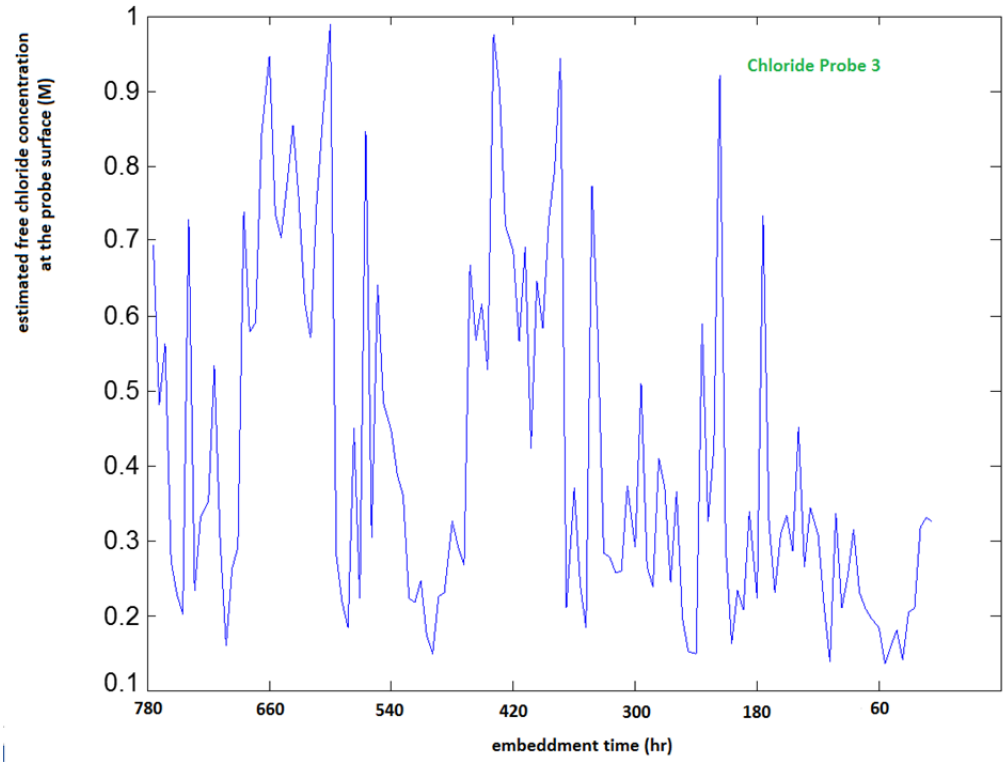

c) Chloride Probe 3

Figure 3.9: Estimated free chloride concentrations at various probe depths inside the field concrete bridge pier a) probe 1; b) probe 2; and c) probe 3.

Figure 3.10 illustrates the temporal evolution of measured average and maximum galvanic current flowing between the pins of the MAS probe 1 inside the field concrete bridge pier. Three main patterns can be seen from these online corrosivity probe readings. First, there are great fluctuations of galvanic current readings, for both the average and maximum corrosion rate of the MAS probe, which may be attributable to the wet/dry cycling inside the concrete. Second, despite the periodical fluctuations, there seems to be an overall trend of peak average galvanic current near 1200 pA (despite the presence of some electronic clipping that led to the flat peaks), which can be translated to maximum average corrosion current density of approximately 0.16 μA/cm2 (considering the exposed surface area of each pin at about 0.0075 cm2), or 1.85 μm/y. As this corrosion current density falls between 0.1 μA/cm2 (upper limit indicative of the passivation of steel) and 1.0 μA/cm2 (lower limit indicative of the active corrosion of steel), the mortar/concrete environment surrounding the MAS probe 1 was relatively corrosive but active pitting of rebar had not initiated yet. The peak maximum galvanic current at the MAS probe 1 was approximately 6000 pA, which corresponds to maximum of maximum corrosion current density of approximately 0.8 μA/cm2 (or 9.27 μm/y). While not presented here, the measured average and maximum galvanic current flowing between the pins of the MAS probe 2 inside the field concrete bridge pier showed similar patterns and similar peak average and peak maximum values as those of the MAS probe 1. Third, during the months of field monitoring, the peak average and maximum corrosion rates did not significantly increase over time, despite the observed overall trend of free chloride concentration increase with time (see Figure 3.9). A moisture sensor at the same location of each MAS probe might help clarify the effect of moisture level on the corrosion rates of the steel inside the concrete.

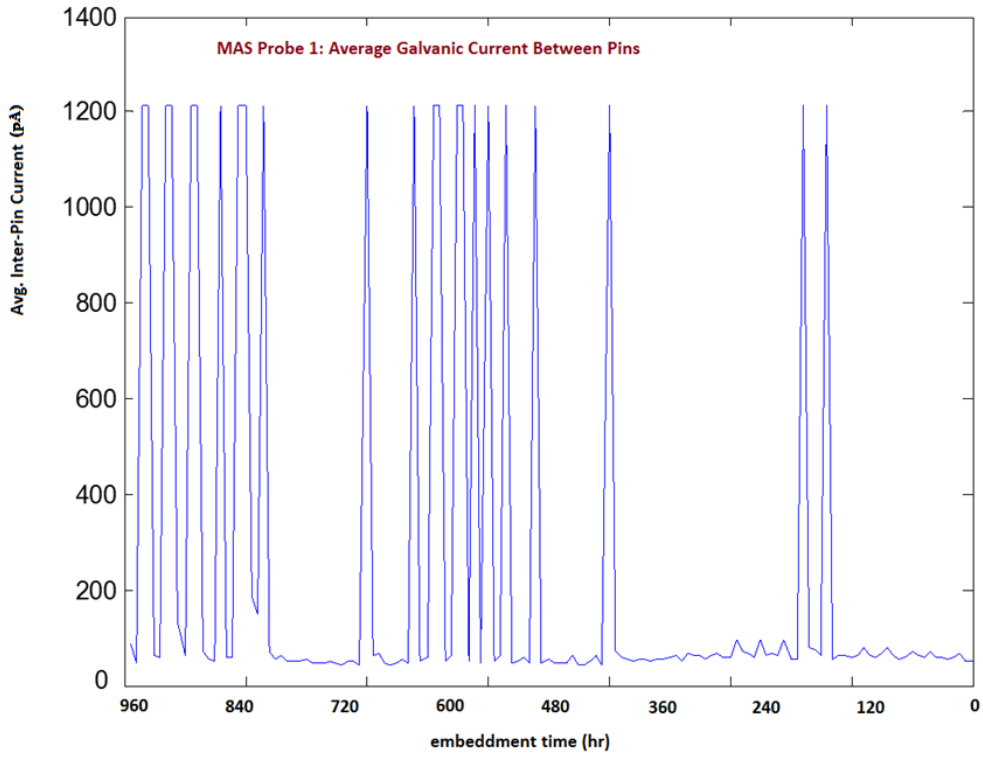

a)

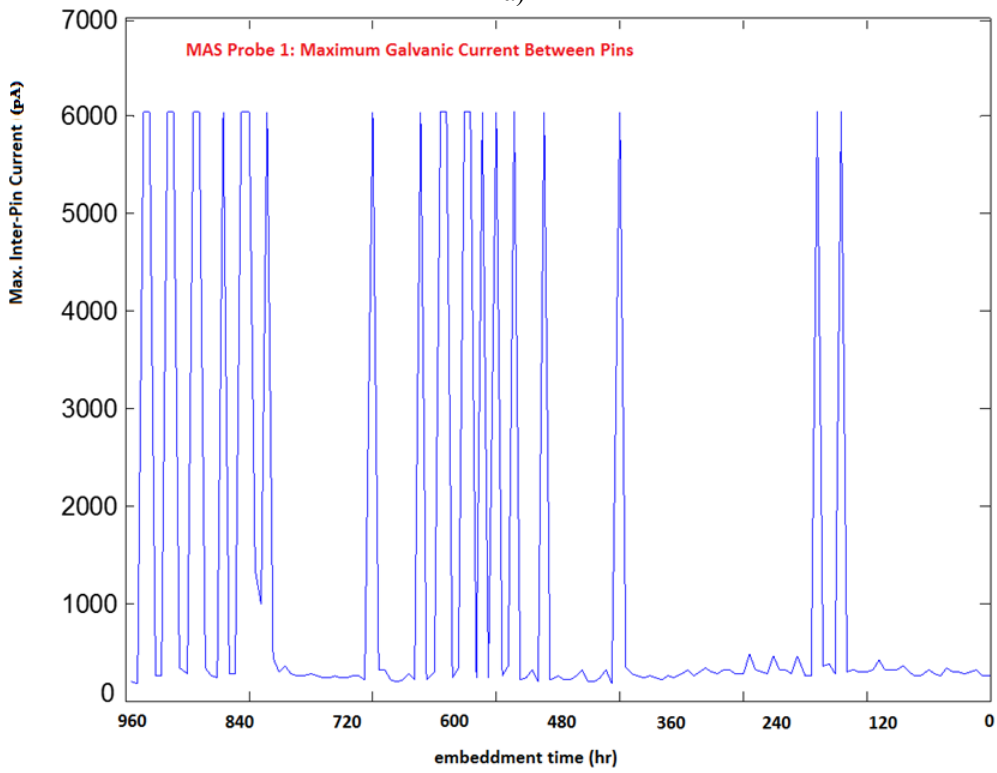

b)

Figure 3.10: a) Average and galvanic current measured; b) maximum galvanic current measured by MAS probe 1 inside the field concrete bridge pier over time

A statistical correlation was explored for the measured maximum galvanic current (ADC_MAX) and the estimated free chloride concentration (SENSOR1CL) at the same time and same sensor depth in concrete. The results are shown below, (Table 3.2), indicating no significant correlation between the two parameters at the depth of probe 1.

Table 3.2. Results of statistical correlation for ADC_MAX and SENSOR1CL

		ADC_MAX	SENSOR1CL
ADC_MAX	Pearson Correlation	1	0.213*
	Sig. (2-tailed)		0.012
	N	139	139
SENSOR1CL	Pearson Correlation	0.213*	1
	Sig. (2-tailed)	0.012	
	N	139	139

Similarly, the same analysis was run for the ADC_MAX and SENSOR2CL. The results are shown below in Table 3.3, indicating no significant correlation between the two parameters at the depth of probe 2.

Table 3.3. Results of statistical correlation for ADC_MAX and SENSOR2CL

		ADC_MAX	SENSOR2CL
ADC_MAX	Pearson Correlation	1	0.004
	Sig. (2-tailed)		0.980
	N	48	48
SENSOR2CL	Pearson Correlation	0.004	1
	Sig. (2-tailed)	0.980	
	N	48	48

4.0 CONCLUSIONS AND SUGGESTED RESEARCH

4.1 CONCLUSIONS

This study has evaluated in the laboratory a multi-parameter corrosion monitoring system for existing reinforced concrete structures in chloride-laden service environments. The study improved and validated the SwRI corrosion sensor prototype for use in the concrete corrosion monitoring system; developed algorithms for quality control and interpretation of the sensor data; made viable recommendations to implement the corrosion monitoring system for existing DOT inventories of RC bridges; and delivered a deployable prototype corrosion sensing system for DOTs to continue field evaluations. The performance and reliability of the SwRI corrosion sensor were confirmed by the benchmark test in simulated concrete pore solutions. However, once active corrosion is initiated and a great amount of chloride is present, the multi-electrode array sensor (MAS) probe may no longer serve as a good tool to predict the corrosion rate of rebar unless more research is conducted to establish such prediction or correlation. The performance and reliability of the SwRI corrosion sensor were also confirmed by embedding it in a paste specimen, while some issues with firmware and possibly the graphite reference probe were identified.

At the WTI laboratory, the custom-made chloride probes along with the SwRI sensor, a conventional Ag/AgCl probe (as control), and three rust-free, bare steel #4 rebars went through a cyclic immersion in the simulated concrete pore solutions. For the 9-pin MAS, the following parameter, standard deviation of maximum ΔE/ average of average ΔE exhibited a very strong correlation with the chloride concentration of the simulated pore solutions. Parameters from the 6-pin MAS probes, such as maximum of maximum ΔE/ average of average ΔE and standard deviation of maximum ΔE/ average of average ΔE exhibited great performance in reliably estimating the chloride concentration and rebar corrosion rate, respectively, even in the case of active corrosion and high chloride concentration.

Only one of the three SwRI Ag/AgCl probes was found to be a reliable chloride probe after the eight cycles of weathering. This highlighted the need for further improving the approach to fabricate the Ag/AgCl probes to serve as chloride probes in concrete. Meanwhile, three WTI custom-made chloride probes (with the appropriate treatment by proprietary coating) showed great promise in this regard. Only one of the three SwRI graphite probes remained relatively stable over the eight cycles of weathering, with its potential showing a standard deviation of 11 mV and a COV of -6%. Interestingly, a few of the WTI custom-made Ag/AgCl probes showed good possibility to serve as reliable reference electrodes in concrete. The majority of the sensing probes featured a response time of less than 60 seconds.

The field demonstration of a corrosion sensing system using the SwRI sensor in the Oregon marine environment revealed key challenges to be addressed in future research, including the need for more weather-proof power supply and electronics as well as better chloride sensors integrated with moisture and temperature sensors.

4.2 SUGGESTED RESEARCH

In light of findings from this study, the following research needs are identified.

- Future research should focus on integration of miniature moisture and temperature probes, enhancing the sensor longevity inside the field concrete, and improving the system reliability, usability and cost-effectiveness.

- Additional research should validate the use of parameters from the 6-pin MAS probes, such as maximum of maximum ΔE/ average of average ΔE, standard deviation of maximum ΔE/ average of average ΔE, or other index calculated from the MAS probe readings (e.g., localized index using the software of electrochemical noise analysis) to reliably estimate the chloride concentration and rebar corrosion rate even in the case of active corrosion and high chloride concentration.

5.0 REFERENCES

Maaddawy, T.E., and K. Soudki. A Model for Prediction of Time from Corrosion Initiation to Corrosion Cracking. *Cement and Concrete Composites*, Vol. 29, 2007, pp.168-175.

Tuutti, K. Service Life of Structures with Regard to Corrosion of Embedded Steel. Performance of Concrete in Marine Environment. *American Concrete Institute*; ACI SP-65, 1980. pp. 223-236.

Weyers, R.E. Service Life Model for Concrete Structures in Chloride Laden Environments. *American Concrete Institute Materials Journal*, Vol. 95, No. 4, 1998, pp.445–453.